Journal of Materials Chemistry A

Accepted Manuscript

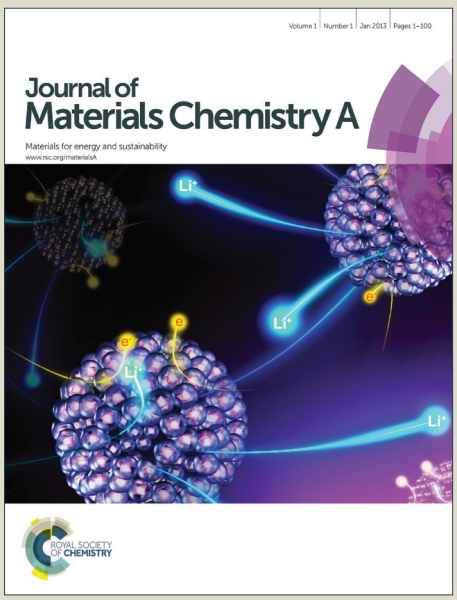

ROYAL SOCIETY OF CHEMISTRY

www.rsc.org/materialsA

High Energy Density Titanium doped-Vanadium Oxide-Vertically Aligned CNT Composite Electrodes for Supercapacitor Applications

Prashanth H. Jampani[a], Oleg Velikokhatnyi[b], Karan Kadakia[a], Dae Ho Hong[b], Sameer S. Damle[a], James A. Poston[c], Ayyakkannu Manivannan[c] and Prashant N. Kumta[a,b,d,e,*]

[a]Department of Chemical and Petroleum Engineering, University of Pittsburgh, Pittsburgh, PA 15261 (USA)

[b]Department of Bioengineering, University of Pittsburgh, Pittsburgh, PA 15261 (USA)

[c]US Department of Energy, National Energy Technology Laboratory Morgantown, WV 26507, USA

[d]Department of Mechanical Engineering and Materials Science, University of Pittsburgh, Pittsburgh, PA 15261 (USA)

[e]Center for Complex Engineered Multifunctional Materials, University of Pittsburgh, Pittsburgh, PA 15261 (USA)

Keywords: Vanadium Oxide; Vertically Aligned Carbon Nanotubes (VACNTs); Supercapacitor; Chemical Vapor Deposition; titanium doped vanadium oxide

Corresponding Author

*E-mail: pkumta@pitt.edu

Abstract

We provide herewith the first report of supercapacitance behavior of titanium doped vanadium oxide films grown on vertically aligned carbon nanotubes using a chemical vapor deposition technique (CVD). The capacitance of CVD derived titanium doped vanadium oxide-carbon

nanotube composites was measured at different scan rates to evaluate the charge storage behavior. In addition, electrochemical characteristics of the titanium doped vanadium oxide thin films synthesized by the CVD process were compared to substantiate the propitious effect of carbon nanotubes on the doped vanadium oxide capacitance. Attractive capacitance values as high as 310 F/g are reported here-in considering the overall materials loading with good rate capability and excellent charge retention up to 400 cycles. Ab-initio theoretical studies demonstrating the substantial improvement in the electronic conductivity of the vanadium oxide due to titanium doping and oxygen vacancies have also been included corroborating the attractive experimental capacitance response.

1. Introduction

The rapid technological progress of the world in the 19th and 20th century could largely be attributed to the extensive use of electricity in the form of small devices such as light bulbs and extending to very large applications such as those powering large mechanical units in industrial plants. In an increasingly dynamic and electronic age however, a large number of mobile applications still rely heavily on mechanical and thermal energy generation and storage which are both inefficient and subject to generation of pollutants. There is therefore, a pressing need for making electricity mobile and this makes it imperative for the development of charge storage devices capable of delivering energy in a manner suiting for a variety of mobile applications such as automobiles and electronic devices i.e. provide energy rapidly over an extended period of time with minimal loss over time[1, 2]. The need to tailor energy storage devices to suit such applications is highlighted by the current targets established by the Department of Energy[3] for the same i.e. 7.5 Wh/kg at 625 W/kg lasting upto 15 years. An examination of the classic Ragone plot will help identify devices capable of achieving the same[4].

It is distinctly observed that only Lithium-ion batteries (LIBs) and electrochemical capacitors have a reasonable propensity to achieve these targets, at least as far as mobile applications are concerned. Electrochemical capacitors often referred to as ultracapacitors or supercapacitors are electrochemical devices which exploit surface charge storage properties of electrode materials, thus enabling rapid charge-discharge and rendering them very attractive for high rate mobile applications such as automobiles and electronic devices. Supercapacitors are typically categorized into two classes based on the nature of charge storage at the electrochemical interface[5]. It is common knowledge in electrochemistry that an electrochemical double layer is formed at an electrode-electrolyte interface as a result difference in Fermi energy-levels of electrons in the electrode and the electrolyte. This difference in energy acts as a barrier to electron tunneling from electrode to electrolyte or vice-versa until a certain potential is applied to the electrode. The electrochemical interface thus acts as a nanometer sized 'double-layer' of separated charges resembling a conventional dielectric capacitor[6]. Charge storage devices based on this mechanism are aptly named electrochemical double layer capacitors (EDLCs).

A second class of capacitors is termed as pseudo-capacitors wherein charge transfer is brought about by virtue of reversible Faradaic electrochemical redox reactions undergone by specific electrochemically active elements within a compound or compounds. The nature of the successive reversible electrochemical reactions of these compounds allows the charge storage response of the device to resemble a capacitor[7]. While double layer capacitors are much more reversible and rapid charge storage devices, pseudocapacitors have much higher energy densities while at the same time maintaining moderately high rate capability on account of the simplistic redox reactions occurring at the surface of the electrode. One could therefore envisage hybrid composite materials capable of both very high rate capability and high energy density.

The synthesis of low cost, high energy, high rate hybrid composite materials requires us to identify a high rate double layer material which can be interfaced with a high energy pseudocapacitor material with a synergistic effect occurring as a result of the composite formed by this interaction. Most commonly studied pseudocapacitor electrode materials to date are hydrous ruthenium oxide and manganese oxide, the former limited by the high cost and the latter restricted primarily due to the low energy density, respectively[8-11]. There is therefore an urgent need for identification of economically viable pseudo-capacitor materials exhibiting reliably high energy densities. Transition metal oxides are very attractive for this kind of application on account of their ability to accept variable oxidation states. In addition, they exhibit excellent atmospheric stability even in nanoparticulate form making handling and storage on a large scale a non-issue. Of particular interest to pseudocapacitor applications is the ability of the surface oxide to undergo successive reversible electrochemical reactions as is the case in hydrous Ruthenium oxide [5, 6]. Hydrous Ruthenium oxide is an excellent pseudocapacitor material with the ability to maintain stable capacitances of upto 900 F/g over a large number of cycles[12]. However, the prohibitive cost of noble metal oxides compels the search for alternative oxide materials with similar charge storage characteristics. One such oxide resembling the multiple oxidation states of the metal similar to Ru is vanadium oxide. Vanadium is an element belonging to Group 5 of the periodic table with a half empty d-shell allowing the element to exhibit multiple valence states from +2 to +5.

Vanadium oxide has previously been studied as a material for lithium ion battery cathodes as well and correspondingly, different morphologies of the oxide including nanotubes have been explored. Amorphous and hydrated vanadium oxide has also been studied widely as a viable supercapacitor electrode in lithium and sodium ion electrolytes [13-21]. Amorphous

vanadium oxide gel/carbon composites have demonstrated capacities ~ 360 mAh/gwith very high intercalation rates. Oxide nanotubes on the other hand, have been studied extensively by Nesper et al.[22, 23]as electrode materials using lithium ion electrolytes and have shown great promise. In addition, a class of so called Lithium-ion based aqueous supercapacitors have been identified by Hu et . al. demonstrating capacitances of upto 740 F/g in aqueous LiCl[24-27]. In all these studies, thin oxide films have shown to result in good electrochemical performance on account of the short diffusion lengths for lithium intercalation. Doping of oxides (Mo, Mn, W, Ti, Cu, and Ag) have been previously studied as an excellent pathway to improve electrical conductivity and electrochemical charge storage properties[28-35]. Silver and copper doped oxides have been shown to increase the electronic conductivities by up to 2 orders of magnitude[36, 37]. Ti and W doped vanadium oxide has also been shown to lead to improvement in pseudocapacitor characteristics[38]. Hence, we have chosen Ti doped vanadium oxide as the pseudocapacitor material to be used in the composite hybrid electrode.

The identification of ideal double-layer type capacitor materials to couple with doped vanadium oxide in order to form a hybrid electrode capable of high rates is relatively complex to tackle on account of the plethora of carbon based double layer materials identified by the capacitor community at large[39-41]. The material we choose must be suitable to overcome the low electronic conductivity usually observed in nanoparticulate oxides. We can examine them individually to find suitable support materials for our application needing high rate capability i.e. very high conductivity, capacitor behavior and excellent stability in the voltage of interest. It is also essential to maintain good carbon material loading and good carbon-oxide interface while at the same time avoiding thick oxide film formation on the carbon, making the underlying carbon material substrate effects redundant. Activated carbons are excellent double layer supercapacitor

materials on account of their high surface area and large pore volume[39, 41]. However, they suffer from the problem of wettability, inability to sustain a uniform deposit on the pores of the carbons. In addition, high surface area carbons usually are very porous resulting in poor volumetric capacitance. Another excellent material that has been studied is graphene. Graphene, as the name suggests is a single sheet of graphite which allows for ballistic 1-D transport of electrons leading to electronic conductivities of up to 10^5 S/m in composites made with graphene[42-47]. However, a major problem with using graphene is that the individual graphene sheets are too thin to achieve sufficient loading of the oxide to achieve high energy densities in practical devices.

On the other hand, an excessively thick deposit of oxide would render the graphene sheet redundant as it would not be able to act as an electron channel to most of the oxide material. A better solution then would be to use carbon nanotubes (CNTs) which have very high conductivity on account of the 1-D electron transport. In addition, it is relatively easy to generate CNTs form vertically aligned arrays which would ensure direct contact of each individual CNT with the current collector as well as creating a 3-D architecture which would act as an ideal substrate for oxide growth[48]. Carbon nanotubes are of two types, SWNTs and MWNTs. SWNTs usually demonstrate slightly better electrical properties than MWNTs[49]. However, the synthesis of pure vertically aligned SWNTs is very expensive and it renders the synthesis of the composite electrodes accordingly prohibitive[49, 50]. In addition, the electronic properties of single wall carbon nanotubes are very much dependent on the nature of the graphene sheets within the nanotube as reported[51-53]. Alternatively, multi-wall carbon nanotubes are relatively inexpensive to synthesize and can be synthesized on a variety of substrates.

Carbon nanotube based hetero-structures have demonstrated improved rate capabilities for various Li-ion and supercapacitor electrode materials including silicon, ruthenium oxide, manganese dioxide and nickel oxide[54-61]. Electrodeposited amorphous hydrated vanadium oxide coatings on CNTs have shown to exhibit capacitances as high as 910 F/g by Kim et al[14] and Balkus et al.[62] in lithium electrolyte cells. In a recent report Sathiya et al. reported energy storage behavior of oxide coated carbon nanotubes in a Swagelok type cell with a lithium electrolyte and a lithium counter electrode exhibiting capacities as high as 850 mAh/g with up to 60% of the energy storage coming from a capacitive contribution[63]. Vanadium oxide/CNT composites have also been explored for capacitance behavior in aqueous electrolytes and capacitances as high as 400 F/g have been reported [64]. In all these studies, thin oxide films have shown to result in good electrochemical performance on account of the short diffusion lengths for lithium intercalation. The importance of loading and its influence in achieving attainable capacitance in vanadium nitride based supercapacitor has been highlighted by us in our earlier work[65]. A recent critical review by Gogotsi et. al. has identified the need to understand the importance of thick films for commercial supercapacitor electrodes and the need to report volumetric capacitance along with gravimetric capacitance[66]. Nanoparticulate materials such as oxides/nitrides of transition metals are very advantageous in terms of achieving desirable electrochemical performance on account of the high specific surface area (SSA) and the enhanced activity that is achievable at the nano-scale dimensions. However, the very fact of having a nanoparticulate state which is responsible for enhanced electrochemical activity results in loss of electronic conductivity on account of the large number of grain boundaries. Nanostructured vanadium oxide has a relatively low electronic conductivity [36, 67, 68] on the order of 10^{-6}-10^{-2} S/cm. The high electronic conductivity of carbon nanotubes (CNTs) on the other hand, could thus be exploited to create composite 3-D

architectures to minimize the oxide–oxide particle contact leading to efficient electron transport from the current collector to the surface of the vanadium oxide wherein the pseudocapacitance behavior is exhibited.

In order to achieve this, architecture comprising vertically aligned carbon nanotubes (VACNT) covered with electrochemically active doped-vanadium oxide would be ideal to obtain maximum capacitance while allowing for slight expansion/contraction likely as a result of the ensuing possible phase change. **Figure 1** shows the various architectures commonly used for supercapacitor applications and their accompanying problems. Previous studies have shown the effect of oxide-film thickness on the capacitance of vanadium oxide films prepared using atomic layer deposition[69]. Thicker films of the oxides however do not yield good charge storage behavior due to the expected limitation in electronic conductivity. The aim in this study is therefore to demonstrate a CNT-oxide composite material wherein the use of a moderately thick doped oxide coating on a forest of vertically aligned electronically conducting carbon nanotubes should allow for minimum electron transport limitations while maximizing active material use and reducing inactive phase weight. This should be reflected accordingly as significant improvement in areal capacity, a measure that is more relevant and of higher consequence than gravimetric capacity.

Morphology	Characteristics
Nanoparticle film 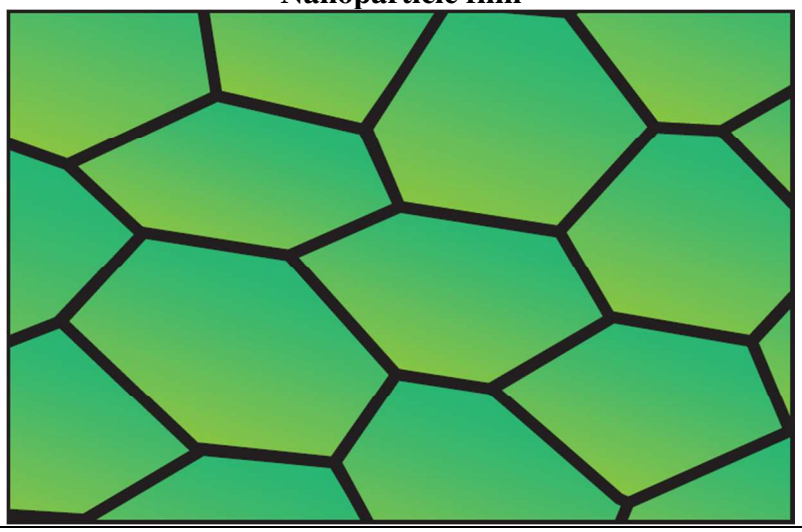	(a) High surface area (b) Poor electronic conductivity (c) Large number of grain boundaries limiting flow (d) Inherently low conductivity of oxide materials hampered further
Thick oxide matrix on carbon nanotubes/CNT-oxide mix film. 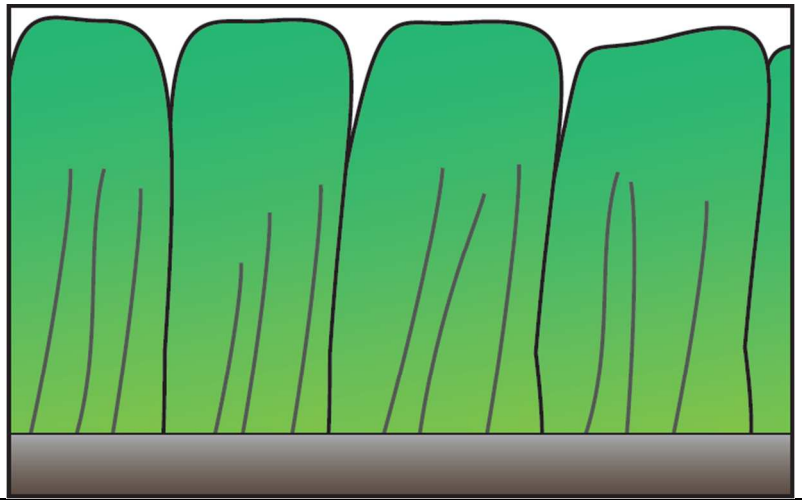	(a) Carbon nanotubes ineffective in reaching all parts of the oxide resulting in large grains and number of grain boundaries (b) Acts like thick film of oxide alone with little conduction of electrons to grains far from CNTs/current collector
Thin oxide coating on vertically aligned carbon nanotube matrix.	(a) Very good electronic contact (b) 3-D architecture ensuring ballistic electron transport to oxide film/grains (c) High oxide-electrolyte

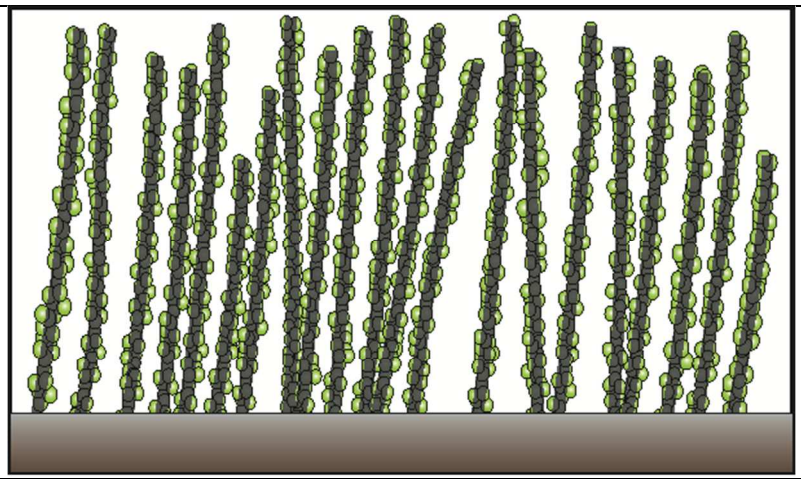	contact maximizing pseudocapacitive contribution (d) Low oxide/CNT weight ratio resulting in low overall capacity when CNTs do not possess significant capacitance (e) Very short diffusion distances from oxide-CNT interface to oxide-electrolyte interface
Moderately thick doped oxide coating on vertically aligned carbon array. 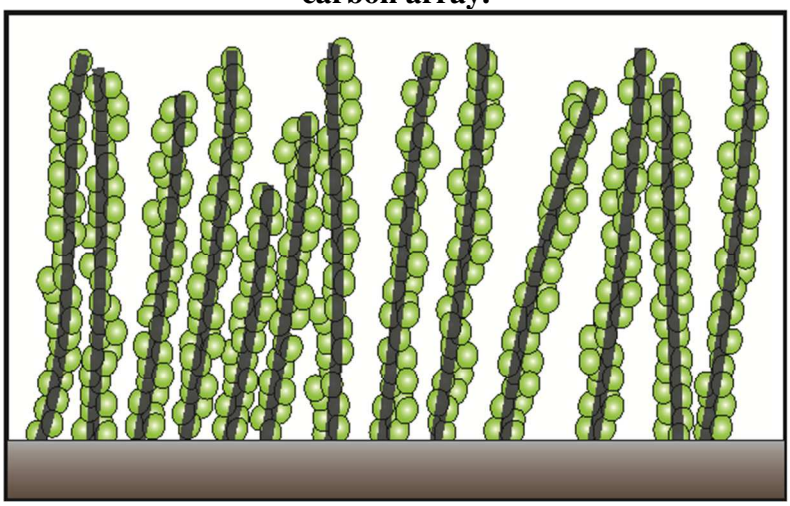	(a) Very good electronic contact between carbon nanotubes and oxide particles (b) 3-D architecture ensuring ballistic electron transport to oxide film/grains (c) High oxide-electrolyte contact maximizing pseudocapacitive contribution (d) Relatively short diffusion distances from oxide-CNT interface to oxide-electrolyte interface (e) Effects of electron mobility reduction due to grains overcome to a large extent by the increased conductivity of the doped oxide (f) Thicker film results in greater oxide/CNT ratio and thus high overall capacitance

Figure 1: Choice of architecture for oxide-CNT composite materials to maximize areal capacitance.

Chemical methods can be utilized to synthesize carbon nanotube-doped oxide composite hybrid electrode materials. However, wet chemical methods usually do not afford the freedom for tailoring the morphology of the composite electrode as thickness of oxide film deposited on the carbon nanotubes is usually very high as the oxide usually forms a matrix around the CNTs rather than retaining nanoparticle nature. Synthesis of Ti doped oxide has usually involved the sol-gel method which is non-ideal for obtaining thin films on carbon nanotubes[70]. This leads to increased oxide-oxide particle contact rather than carbon-nanotube-oxide electron transport. In addition, carbon nanotubes usually need to be dispersed in an oxide sol, leading to loss in alignment of the CNTs. The very purpose of using CNTs i.e. one dimensional transport of electrons to nano-sized film of the oxide is lost. Chemical vapor deposition (CVD) is an ideal and versatile method to obtain uniform architectures on carbon structures [71, 72] while also tailoring the nature of the deposited film depending on the deposition conditions. Various groups have previously reported CVD as a technique for the growth of vanadium oxide thin films[54, 73-79] using both chloride and metal organic precursors. Oxide films with varying V oxidation states have been reported with ratios of oxides depending on the various deposition conditions including temperature and reagent concentrations[78].

Though some improvement in electronic conductivity and evidence of improvement of charge storage by doping of oxides has previously been demonstrated, a detailed fundamental study has not been undertaken correlating supercapacitor behavior with doping in both nanoparticulate oxide and nitride materials. On the basis of the existing evidence in literature, it is to be expected that a first principles computational screening study to identify suitable dopants could be used to predict and engineer high capacity, high rate, and stable supercapacitor materials. The aim of this work is thus to use doping of oxides as an approach that allows for

modifying the electronic conductivity and thus the electrochemical activity, as well as the electrochemical stability of nanoparticulate oxides and nitrides. Using a theoretical simulation involving d-band assessment of the structure, suitable dopants have been identified to improve the electronic conductivity and thus the supercapacitor behavior of nanostructured oxides. Using such approaches, the current study provides a unique methodology for generating thick film architectures of doped vanadium oxides grown on vertically aligned CNTs (VACNTs) resulting in capacitance values that are uniquely distinct from currently reported values in the literature. Accordingly, in this work, an atmospheric pressure chemical vapor deposition (APCVD) method has been explored to deposit titanium doped-vanadium oxide on vertically aligned carbon nanotubes for use as a supercapacitor electrode in aqueous media. Implementation of CVD as a synthesis method also provides the advantage of avoiding the incorporation of binders for generating the electrodes which can consume upto 50% of the total weight of the electrode in high surface area systems contributing largely to inactive dead weight[55, 72]. As a result of the improved electronic conductivity of doped vanadium oxide and high conductivity of vertically aligned carbon nanotubes, we are able to demonstrate high gravimetric capacitances in thick electrodes resulting in high areal capacities.

2. Experimental Methods

2.1 Materials Synthesis

2.1.1 Chemical Vapor deposition

A two-step CVD process was used to obtain doped-vanadium oxide nanosphere coated CNT hetero-structures on nickel substrate disks. First, the nickel disks were properly cleaned using dilute acids and acetone, and then weighed. Vertically aligned carbon nanotubes

(VACNTs) were then deposited on the Ni disks (Alfa Aesar Inc., 0.05 mm thick, annealed, 99+% (metals basis)) using a xylene-ferrocene mixture following a hot wall chemical vapor deposition (CVD) procedure similar to that reported by Ajayan et al. using an Ar/H_2 mixture[80, 81]. m-Xylene (ACROS organics, extra pure, >99%) was used as the carbon source with ferrocene (ACROS Organics, 98%) acting as the catalyst for CNT nucleation and growth (**Figure 2a**). The mixture was vaporized and led into a hot-wall CVD tube maintained at 770° C. Deposition was carried out for 30 minutes resulting in the growth of a uniform forest of vertically aligned carbon nanotubes. The VACNT coated Nickel disks were then weighed and a low temperature hot-wall APCVD setup was used to deposit the doped vanadium oxide directly onto the vertically aligned carbon nanotubes. To generate the doped vanadium oxide, appropriate mixtures of vanadium tetrachloride (VCl_4, Sigma Aldrich) and metal dopant introduced as a chloride precursor, i.e. titanium tetrachloride ($TiCl_4$, Sigma Aldrich, 99.9% metals basis) were dissolved in an aprotic solvent, chloroform ($CHCl_3$, ACROS Organics, 99.9% Extra dry) in an inert atmosphere glove box (Vacuum Atmospheres Inc.: model EE-493, below 5ppm O_2 + H_2O) and recovered in a sealed stainless steel evaporator bottle.

The doped vanadium oxide nanospheres were deposited on the VACNTs using a hot wall tubular APCVD setup (**Figure 2b**) consisting of two separate nitrogen (UHP N_2, Grade 5, Valley National gas) carrier gas lines running through the evaporator vessels, one containing the mixture of chloride precursors and another containing a distilled water (Millipore QGARD, Resistivity=18.2 MΩ-cm) line driven by a syringe pump (Thermo Scientific Orion M365 Sage syringe pump). Both precursors were evaporated and carried into a hot wall CVD reactor tube wherein the CNT coated nickel (Ni) disks were placed[17, 38, 78, 82-84]. Deposition was carried out at 250°C for 20 minutes. The oxide coated disks were then weighed and characterized. Doped

Vanadium oxide thin film was also generated by depositing the doped oxide directly on the Ni substrate disks by CVD using the same precursors to compare the electrical and electrochemical properties of the thin films of the doped oxide with that of the composite heterostructure comprised of doped oxide coated on VACNTs.

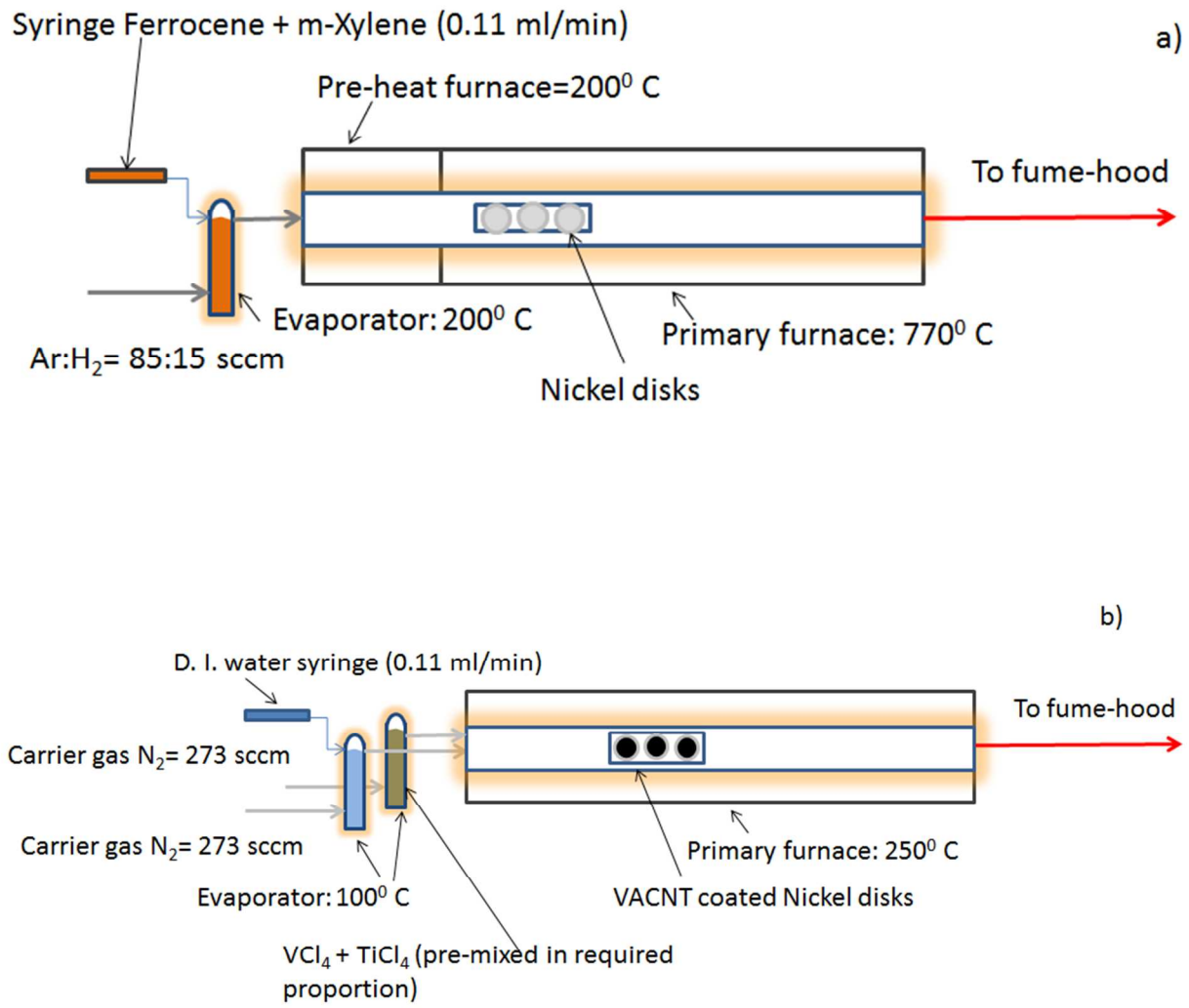

Figure 2: Chemical vapor deposition setup for deposition of (a) VACNT forest (b) VO_x:Ti-VACNT composite.

2.2 Materials Characterization

The nature of the deposit including morphology of the oxide on the CNTs needs to be analyzed and examined to obtain a better understanding of the observed capacitance behavior. To accordingly investigate and compare the microstructure of the CVD deposited doped vanadium oxide-CNT composites and thin films, scanning electron microscopy (SEM) analysis was conducted using a Philips XL30 machine operating at 20 kV. The atomic composition of the films was also verified using EDAX analysis. To study the nature of the doped oxides coated on the CNTs and to identify presence of any amorphous deposits other than the oxide present on the CNTs, micro-Raman spectroscopy was performed on a Reinshaw inVia Raman microscope. Raman spectra were collected in air at room temperature using a 633 nm laser. Low laser intensities were chosen to avoid beam modification of the samples and accordingly, the spectra were collected by averaging multiple scans over a frequency range of 3500-100 cm^{-1}.

To further characterize the doped oxide-CNT interface and morphology of the doped oxides, high-resolution transmission electron microscopy (HRTEM) was performed on a JEOL JEM-210F microscope using beam energy of 200 keV. Samples for HRTEM were prepared from the CVD synthesized composites by scraping off the doped vanadium oxide deposited VACNTs from the Ni substrate, followed by suspending in methanol and dispersing them on to 3.05 mm diameter Nickel grids (JEOL, 400 mesh nickel) containing a holey carbon film by sonication. The grids were then vacuum-dried for 24 h and subjected to conventional and HRTEM analyses.

X-ray photoelectron spectroscopy (XPS) was performed on a Perkin-Elmer PHI-5600 ESCA system to analyze the surface composition and determine the valence state of V ions in the oxide-VACNT composite. XPS was conducted using a Physical Electronics (PHI) model 32-096

x-ray source control and a 22-040 power supply interfaced to a model 04-548 x-ray source with an Omni Focus III spherical capacitance analyzer (SCA). The system is routinely operated within the pressure range of 10^{-8} to 10^{-9} Torr (1.3×10^{-6} to 1.3×10^{-7} Pa). The system was calibrated in accordance with the manufacturer's procedures utilizing the photoemission lines, E_b of $Cu_{2p}^{3/2}$ - 932.7 eV, E_b of $Au_{4f}^{7/2}$ - 84 eV and E_b of $Ag_{3d}^{5/2}$ - 368.3 for a magnesium anode. All the reported intensities are in effect experimentally determined peak areas divided by the instrumental sensitivity factors. Charge correction was obtained by referencing the adventitious C_{1s} peak to 284.8 eV.

The electronic conductivity is a crucial parameter affecting the supercapacitor performance and hence, four point probe conductivity set up was used to measure the conductivity of the vanadium oxide films prepared by CVD. A Veeco FPP 5000 four-probe conductivity instrument (Miller Design & Equipment, Inc.) was used for the conductivity measurements and the sheet resistance values obtained were then converted to electrical conductivity. Four-probe conductivity data is usually obtained by preparing pellets from powders and supporting them on insulators while maintaining contact with four equally spaced probes, two of which supply current while the other two measure voltage across them following standard known procedures. The measurement of resistivity of thin films deposited on conducting metal substrates however is a difficult proposition as the flow of electrons from the two current probes would probably occur through the substrate current collector itself offering the least resistance path. This current flow does not however occur in the CVD derived doped oxide and the VACNT- doped oxide composite as the deposit is sufficiently thick and crack free to avoid interference from the substrate.

2.3 Electrochemical Testing

Cyclic voltammetry (CV) was performed on the synthesized doped vanadium oxide thin film and doped vanadium oxide-VACNT heterostructure materials to test their viability as high energy density supercapacitor materials. A three electrode cell configuration was used to perform cyclic voltammetry measurements and electrochemical impedance spectroscopy analysis (EIS) on the coated Ni disks to both understand the electrochemical mechanisms involved as well as evaluate the specific capacitance of both, the VACNT- doped vanadium oxide nanosphere composite, and the doped vanadium oxide thin films prepared by chemical vapor deposition. The cell was assembled using platinum as the counter electrode, Ag/AgCl (in 3M KCl) as the reference electrode, and the active material coated Ni disks described above as the working electrode. An aqueous 1M Na_2SO_4 solution was used as the electrolyte.

Cyclic voltammetry tests were performed on a Princeton Applied Research (PAR) Versastat-3 potentiostat in the -1 V to 0.8 V potential ranges with respect to the reference electrode to evaluate the specific capacitance of the doped vanadium oxide-VACNT composite heterostructures generated by CVD. It was observed that no significant water electrolysis occurred in this extended voltage window. Cycling was therefore performed at different scan rates and area of the cyclic voltammogram was used to calculate the total capacitance. Gravimetric capacitance values were evaluated on the basis of both the oxide weight alone as well as the weight of the total active material.

The capacitance was calculated using the formula:

$$\text{Capacitance C (in F/g)} = \frac{\int I\, dV}{s*2*V*m} \qquad \text{i);}$$

where

$\int I\, dV$ = area generated by cyclic voltammogram

s= scan rate in V/s,

V= voltage window =1.8 V,

and m= mass of the active material in gram.

In addition to cyclic voltammetry, galvanostatic charge-discharge cycling was performed on an Arbin BT-2000 cycler at different current densities in the voltage window of -0.5 to 1 V w.r.t Ag/AgCl (3M KCl) to observe the nature of the voltage-time (V-t) characteristic and to obtain capacitance values under galvanostatic conditions which resembles more closely commercial applications of supercapacitors. The capacitance accordingly was calculated by integrating the current-time data over the voltage window.

To further evaluate the supercapacitor response of the CVD-deposited doped vanadium oxide thin films, doped vanadium oxide-VACNT heterostructures, electrochemical impedance spectroscopy was performed on the Applied Research (PAR) Versastat 3 over a frequency range of 0.1Hz-100 KHz. A 5 mV amplitude was used and the spectra were collected between -1.0 and 0.8 V at the specific voltages where Faradaic reactions were observed to be predominant. Impedance spectroscopy is a versatile technique which can be used to quantify charge transfer parameters in electrochemical systems. The impedance spectra were obtained on the titanium doped vanadium oxide thin film and the VACNT-titanium doped vanadium oxide nanosphere composite heterostructure hybrid electrodes to observe any noticeable changes in charge storage mechanism induced by the presence of carbon nanotubes. The ZView-2 (Scribner Associates, Inc.) software was used for theoretical modeling and fitting using the Randall's equivalent circuit models, and the charge transfer parameters corresponding to the CVD synthesized doped

vanadium oxide-VACNT nanostructures were obtained and correspondingly compared to the doped oxide thin film to understand the effect of VACNTs on the performance of the Ti doped vanadium oxide.

3. Results & Discussion

Figure 3a shows the scanning electron microscope (SEM) image of vertically aligned CNTs (VACNTs) deposited by chemical vapor deposition on Ni substrate using a deposition time of 30 minutes for growth of carbon nanotubes. The carbon nanotubes grow on the nickel substrate supported by iron nanoparticles (from Ferrocene) which nucleate on the surface of the nickel as islands and in turn acting as growth sites for carbon[85, 86]. The carbon then grows in the form of nanotubes by progressive rise of the nucleated iron islands which continue to act as nucleation sites (floating catalyst mechanism) of carbon. Hence the length of the tubes can be controlled by varying the CVD deposition time. Accordingly, optimized deposition time of 30 minutes was used to obtain the vertically aligned tubes 120 micron in length. The hypothesis is that the prolific length of the CNTs would help create a very good 3-D architecture which when covered with a thin layer of the oxide would maximize the volumetric loading while at the same time ensuring that a very thick film does not cover the entire surface of the carbon nanotubes impeding electronic transport within the oxide itself.

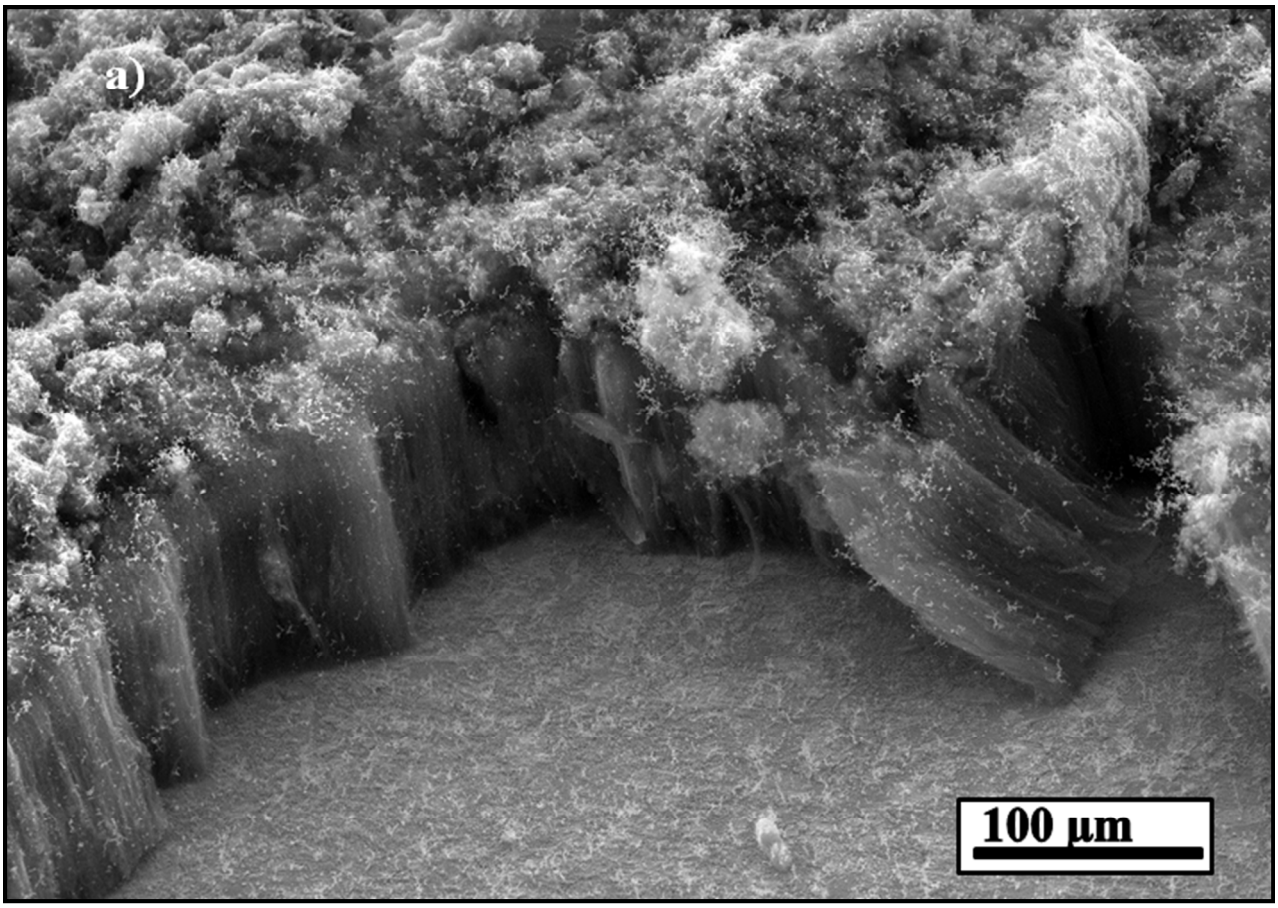

Figure 3b shows the SEM image of titanium doped vanadium oxide (VO_x:Ti) coating on the vertically aligned CNTs deposited by chemical vapor deposition using the pre-mixed chloride precursors and water which were aspirated using the CVD system described in **Figure 2b**. Deposition of the doped oxide using the pre-mixed chloride precursors and water aspirated in the CVD system was carried out for 20 minutes ensuring that the oxide is coated on the VACNTs in the form of a contiguous film consisting of a number of nanometer sized globules. **Figure 4** shows the bright field high resolution transmission electron microscopy (HRTEM) image of VO_x:Ti-VACNT hybrid composite scrapped off the nickel substrate. The image confirms that the VO_x:Ti is deposited over the VACNTs in the form of a semi-contiguous film consisting of ~250

nm diameter amorphous globules evident by the lack of visible lattice fringes in the oxide particle seen in **Figure 4**.

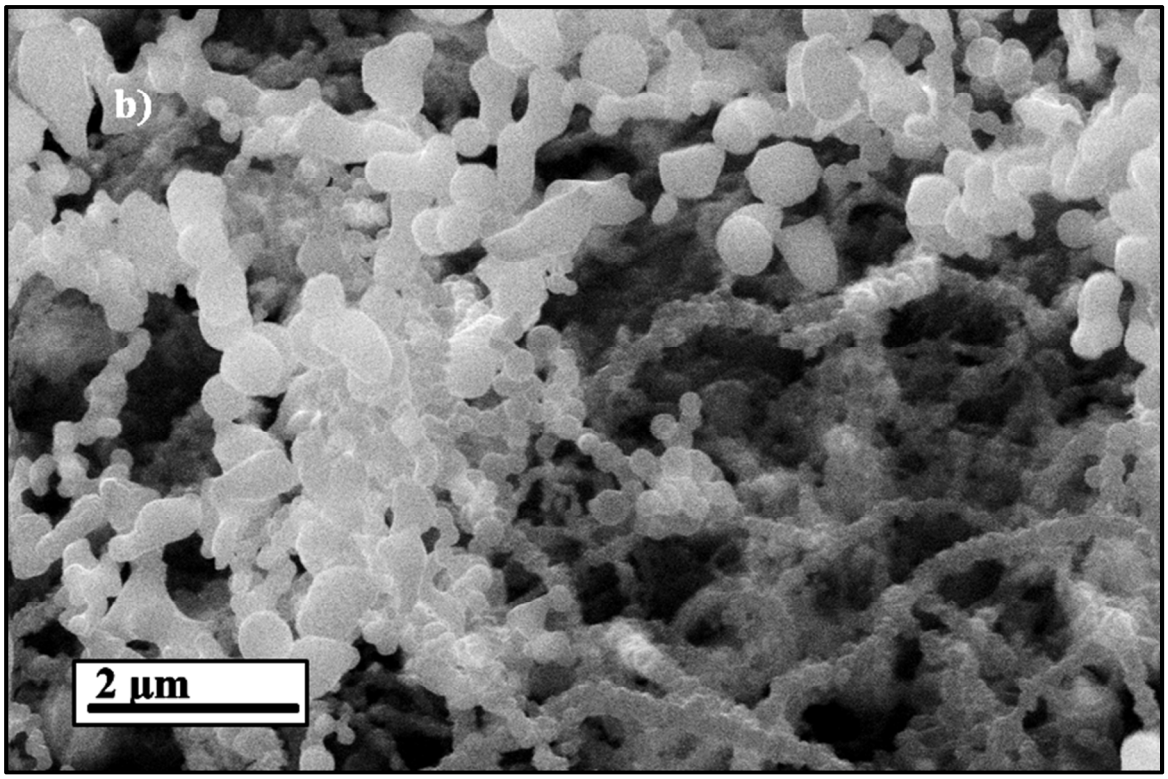

Figure 3: Scanning Electron Microscope image of (a) CVD derived Vertically Aligned Carbon nanotubes coated with titanium doped vanadium oxide showing forest of vertically aligned carbon nanotubes, and (b) Nanoparticulate titanium-doped vanadium oxide coated on the carbon nanotubes grown by chemical vapor deposition.

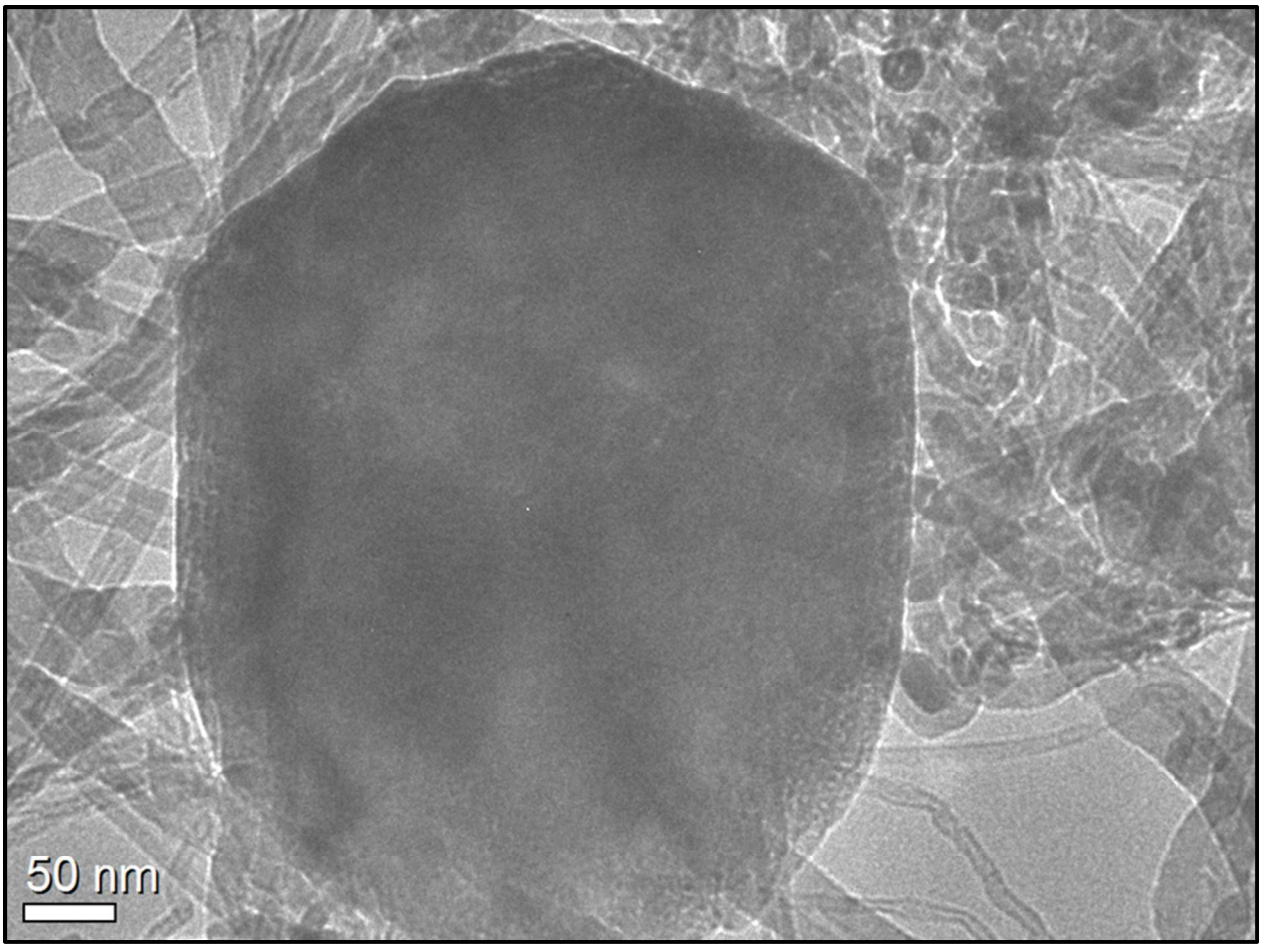

Figure 4: HRTEM images of the VO_x:Ti coated on the vertically aligned carbon nanotubes (VACNTs) showing nanoparticulate size of the oxide particles grown on the carbon nanotubes.

Energy dispersive x-ray analysis (EDX) was performed on the sample as shown in **Figure 5** since the composition of the CVD derived VO_x:Ti-VACNT could not be accurately confirmed by x-ray diffraction due to the amorphous nature of the oxide deposited on the VACNTs (**Figure 4**). The presence of elemental V, O and Ti in the VO_x:Ti-VACNT heterostructures has been confirmed using the EDX configured to the SEM. The V and Ti ratio in the VO_x:Ti-VACNT is similar to the nominal composition used and is confirmed by EDX. Nickel is also observed in the EDX which is due to the substrate on which VO_x:Ti-VACNT is

synthesized. It was found that the CVD derived doped oxide-VACNT composite heterostructure had a nominal composition of $V_{1.6}Ti_{0.4}O_{5-x}$ with x ~ 0.4. The vacancy rich oxide thus formed would correspond to a high oxidation state of vanadium which has previously been identified to be essential for achieving high capacity in vanadium oxide [24, 87].

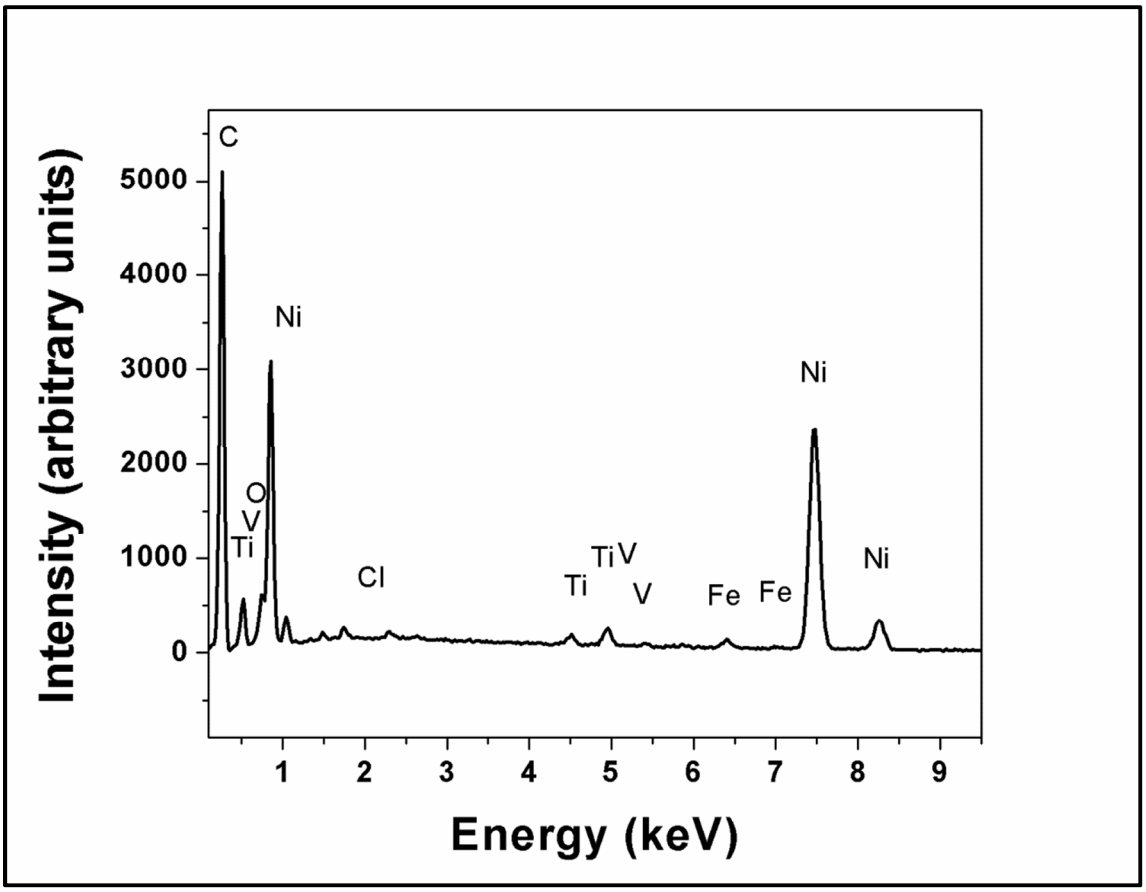

Figure 5: EDX spectra of the VO_x:Ti -VACNT composite heterostructures synthesized by CVD.

In order to determine the chemical oxidation states of V, Ti and O in the VACNT-doped oxide composite electrode, x-ray photoelectron spectroscopy (XPS) was conducted using a Phillips PHI 5600 system. The XPS spectra of V_{2p} and O_{1s} peak of vanadium oxide obtained are shown in **Figure 6**. As shown in the figure, the binding energy of vanadium [$V_{2p}^{3/2}$ (516.95 eV) and $V_{2p}^{1/2}$ (524.49 eV)] is indicative of V in the oxidation state between +4 and +5[88, 89]. Further,

reported $V_{2p}^{3/2}$ values of vanadium oxide for the +4 oxidation state i.e. VO_2 vary between 515.7 and 516.5 eV, and for the +5 oxidation state i.e. V_2O_5 vary between 514.9 and 518.3 eV. Therefore an oxidation state of +4/+5 has been attributed to the vanadium in this study[90]. The binding energy of titanium [$Ti_{2p}^{3/2}$(458.51 eV) and $Ti_{2p}^{1/2}$(463.83 eV)] in the CVD derived VACNT-doped oxide corresponds very closely to Ti existing in the stable +4 oxidation state[76]. The binding energy of oxygen O_{1s} (529.96 eV) corresponds to a high oxidation state of the metal, namely in the +4/+5 oxidation state. Both the vanadium and titanium are thus in their highest oxidation states which is conducive for achieving the observed and improved supercapacitor response reported herein. Further analysis including deconvolution of XPS peaks has not been undertaken herein since XPS results have been used only as an indicator of the presence of a mixed oxide of vanadium and titanium in the VO_x:Ti -VACNT composite heterostructure. The Ti doped vanadium oxide coated on the VACNTs synthesized by the CVD approach exhibits V displaying a mixture of high oxidation state of V^{5+}/ V^{4+} similar to that of other promising oxide systems used in supercapacitors[24, 87]. The XPS spectrum and binding energies thus match very closely that of Ti doped vanadium oxide reported earlier [91].

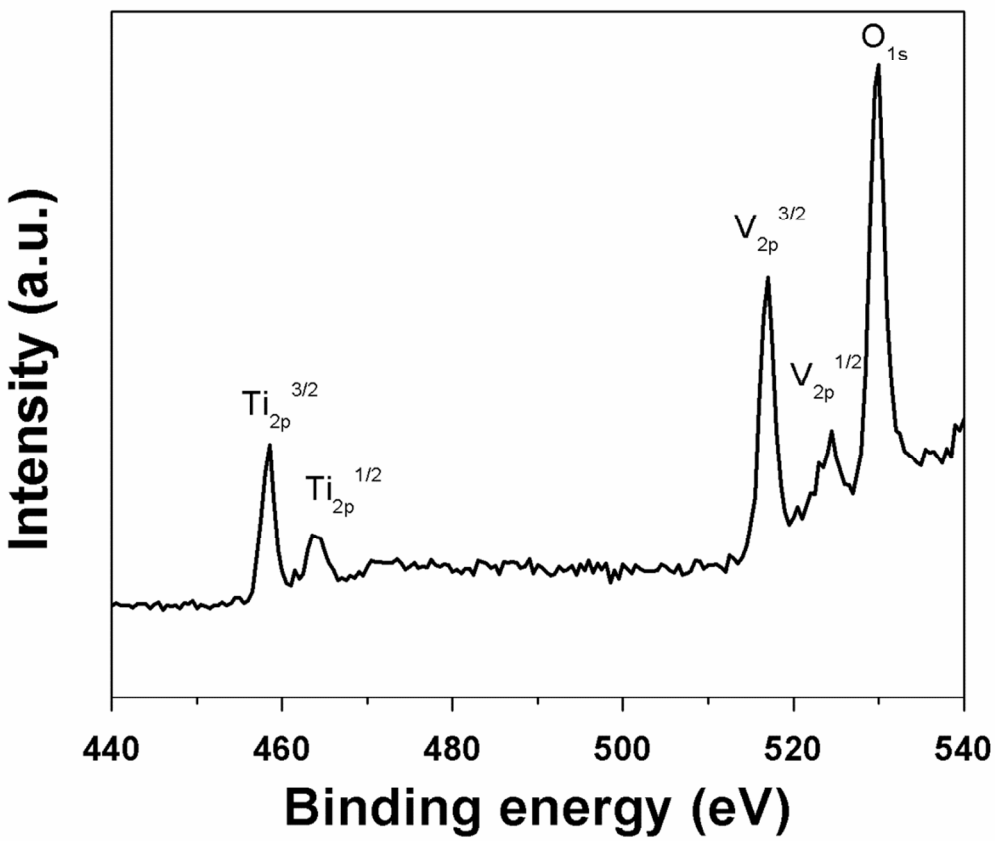

Figure 6: X-ray photoelectron spectrum of CVD deposited VACNT-titanium doped vanadium oxide composite heterostructure showing the peaks corresponding to the binding energies of vanadium, titanium and oxygen.

Raman spectra was collected on the VO_x:Ti-VACNT which is shown in **Figure 7a** since the x-ray diffraction pattern of the titanium doped vanadium oxide could not be acquired on account of the amorphous nature of the oxide grown on the VACNTs. The D, G and G' bands are observed at 1250, 1650 and 2650 cm^{-1}. The G/D (I_g/I_d=1.16) ratio is greater than one indicating few lattice defects in the graphene layers resulting in MWCNTs with relatively high conductivity[92, 93]. This would also have a positive effect on the capacitance behavior of the Ti doped vanadium oxide. **Figure 7a** shows several peaks marked that have been identified to correspond and match closest

to those observed and reported in thin films of V_2O_5[94] and those of vanadium oxide corresponding to VO_x-carbon nanofibers reported previously[95]. **Table 1** also shows the tabulated peak positions observed in **Figure 7a** and indicates the nature of the vibration resulting in the peaks seen in the Raman pattern of VO_x:Ti-VACNT. The V bonds which are characteristic of double and multilayer structures usually observed in V_2O_5 appeared at 404, 528 and 996 cm^{-1}[96, 97]. The peak at 700 cm^{-1} is indicative of stretching vibration of oxygen ions in bridging position between the three vanadia centers[97]. The peak observed at 477 cm^{-1} is at a similar position to that observed in V_2O_5 where oxygen ions are situated between the two vanadium centers[97]. Titanium oxide conventionally has Raman peaks corresponding to the anatase phase at 142 cm^{-1} (E_g), 395 cm^{-1}(B_{1g}), 515 cm^{-1} (B_{1g}+A_{1g}) and 636 cm^{-1} (A_{1g}). Brookite (TiO_2) on the other hand, usually has a strong band at 153 cm^{-1}(E_g) and another at 320 cm^{-1} (B_{1g})[98, 99]. No Raman lines due to titanium oxide can be observed in the VO_x:Ti-VACNT samples, which proves that the titanium is dispersed very well in a homogeneous manner with no observed phase separation and formation of any random individual titanium oxide clusters. It also confirms that titanium may be present in the substitutional positions in the lattice of the parent vanadium oxide. As seen in **Table 1**, every single peak is seen to match with that of the linkages seen in the vanadia lattice. However, the peak occurring at 830 cm^{-1} does not match any of the vibrations of vanadium and oxygen. Nevertheless, it matches closely with that of V-O-Ti as reported by Krykova et al.[100] (Ti-O-V linkage at a wavenumber of 860 cm^{-1} has been reported). The wavenumber of 830 cm^{-1} also matches that of rutile TiO_2 seen in TiO_2 supported V_2O_5[101]. However, none of the other vibrations of the rutile phase are present leading us to conclude that it is indeed a Ti-O-V bond rather than a secondary rutile phase. Titanium and vanadium have similar ionic radii which allows for the relative ease of doping and substitution of titanium on V sites in the vanadium

oxide lattice. **Figure 7b** shows the comparison of Raman spectra seen in VO_x:Ti-VACNT and VO_x-VACNT. It can distinctly be observed that the peak at 830 cm^{-1} is absent in the VO_x-VACNT further corroborating the hypothesis that the peak position occurs as a result of a Ti-O-V vibration.

Table 1: Peak positions observed in Raman spectrum of VO_x:Ti-VACNT and corresponding vibrations.

Wavenumber (cm^{-1})	**Vibration**	**References**
145	$(V_2O_2)n$, bending	85
197	$(V_2O_2)n$, bending	85
284	V=O, bending	85
304	V_3-O, bending	95, 101
404	V=O, bending	95, 101
477	V-O-V, bending	95
528	V_3-O, stretching	95
700	V_2-O, stretching	95
830	V-O-Ti	96, 100
941	Bridging V-O-V vibrational bands	100-102
992	Symmetric stretching of V=O bond	100, 101
1250	CNT-D-band	78, 79
1650	CNT-G-band	78, 79

2650	CNT-G'-band	78, 79

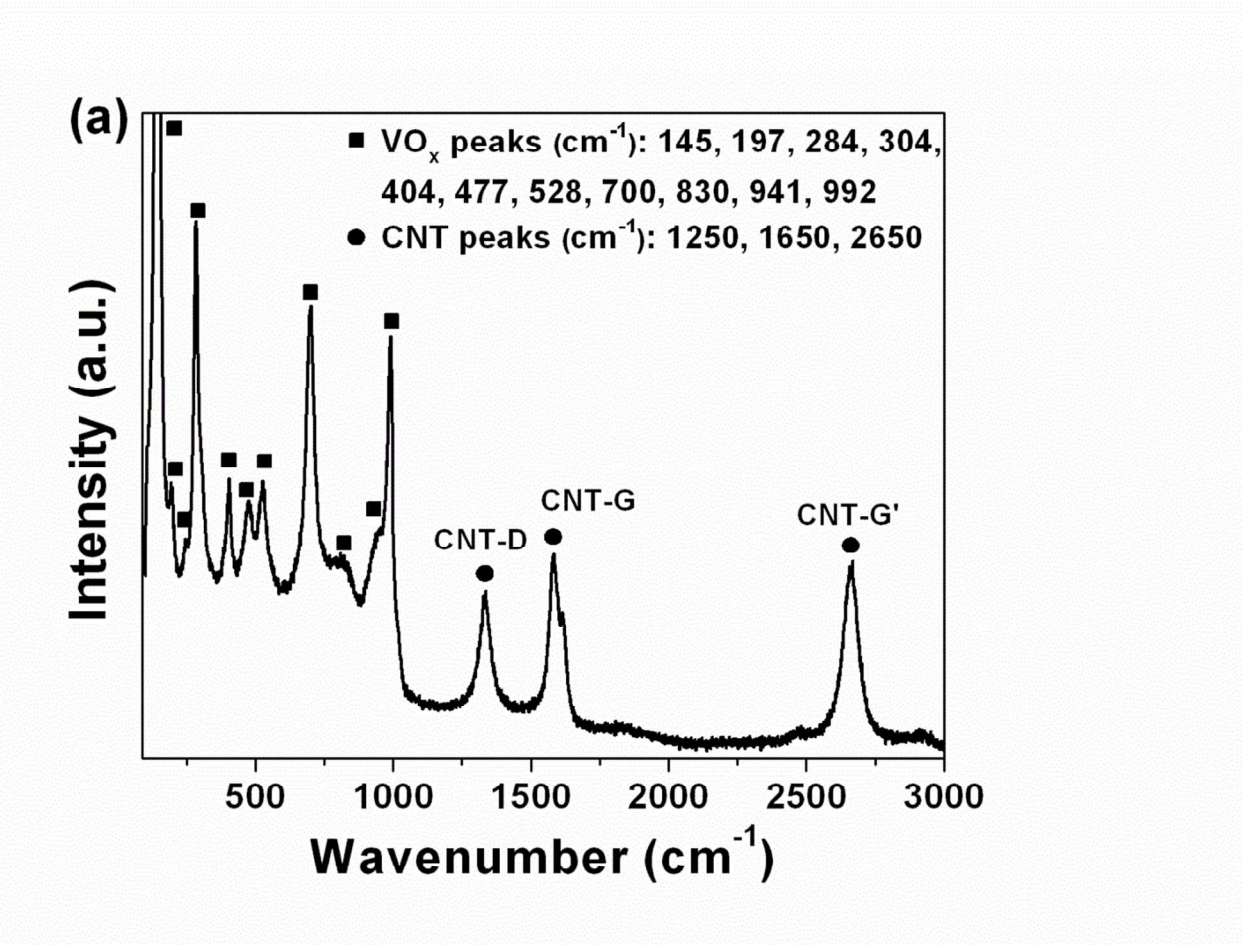

465

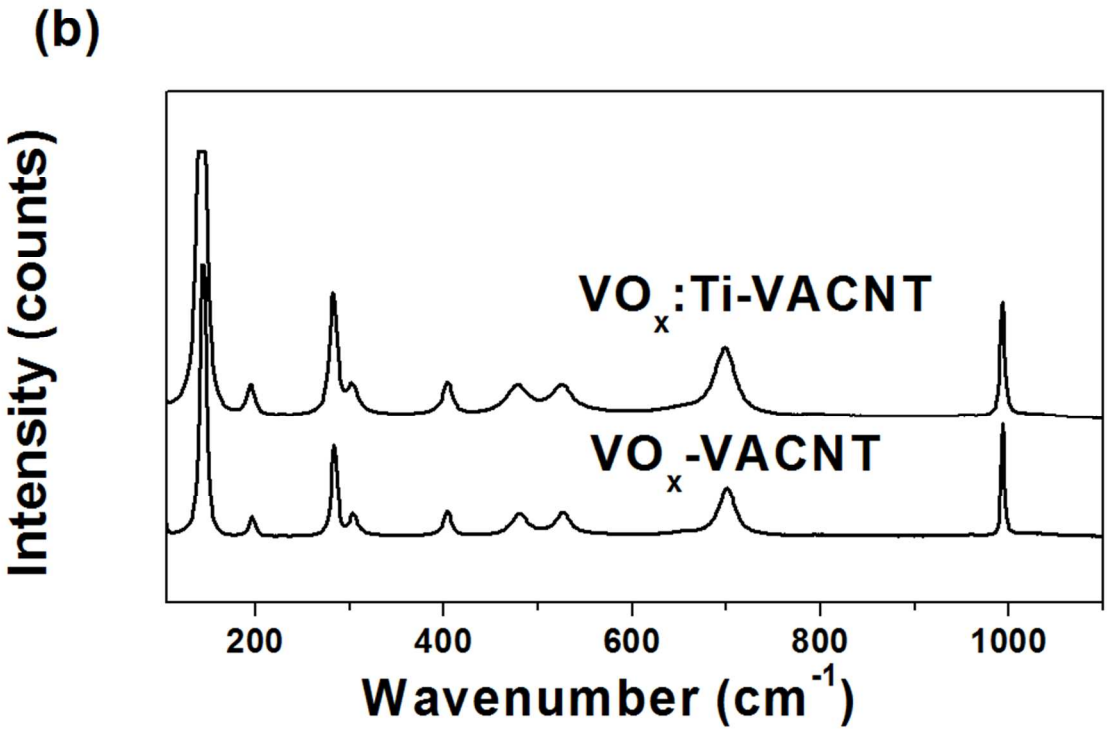

Figure 7: Raman spectra of vertically aligned CNTs coated with titanium doped vanadium oxide (VO_x:Ti-VACNT) over a frequency window of 100-3000 cm^{-1} showing the presence of oxide and CNT peaks (a), and comparison of Raman spectra of CVD derived VO_x:Ti and VO_x coated on VACNTs (b).

Four-probe conductivity measurements were also performed on both the thin film oxide and VACNT-supported VO_x:Ti nanocomposite heterostructures. Sheet conductivity data was obtained using a Veeco- FPP 500 instrument wherein the coated Ni disks were suppressed onto standalone tips and voltage *vs.* current was measured. Sheet resistance data was multiplied with the thickness to obtain bulk resistivity which is reported in **Table 2**. The electronic conductivity of the nickel disk was found to be almost 5 orders of magnitude larger than that of either the VO_x, VO_x:Ti, VO_x-VACNT or VO_x:Ti-VACNT composites indicating that the four-probe

conductivity data does not bear any artifact arising from the current collector. The conductivity values fall within the range of resistivities reported ($10^1$and 10^4 Ω-cm[36, 103]) in the literature for various oxidation states of vanadium at room temperature. As expected, the electronic conductivity of the VACNT supported VO_x and VO_x:Ti is much higher than that of the respective thin film undoped and Ti doped vanadium oxides. The vertically aligned support structure provided by the VACNTs clearly allows for a thin film of oxide to be supported by highly conductive CNTs resulting in more effective transport of electrons through the CNT channels reflected in the improved electronic conductivity. The Ti-doped VO_x supported on VACNT clearly demonstrates the combined benefits of doping as well as the CNT architecture together adding to the improved electronic conductivities even better by more than order of magnitude compared to undoped VO_x supported on VACNTs as seen in Table 2.

The deposition of oxide film on CNTs therefore leads to conductivities similar to those of vanadium oxide nanowires reported previously[104]. In addition, the electronic conductivity of the VO_x:Ti-VACNT can be seen to be almost one order higher than that of the VO_x-VACNT as mentioned above. Moreover, titanium and vanadium have similar ionic radii which allows for the relative ease of doping of titanium into the vanadium oxide lattice. Vanadium doping of titanium oxide has also previously been proposed to result in increased electronic conductivity[100, 105]. The doping of titanium oxide with vanadium substantially changes its properties; i.e., the life time of charge carriers increases[106] resulting in increased electronic conductivity. It is expected that a similar phenomenon would be reflected to occur in the case of titanium doped vanadium oxide as well. Vanadium oxide is a well-known n-type semiconductor [107]. The presence of oxygen vacancies as observed in the EDX data would also contribute to increased electronic conductivity.

It is believed the doping of titanium into the vanadium oxide lattice would result in a vacancy mechanism as proposed in Equation ii.

$$1.6VCl_4(g) + 0.4TiCl_4(g) + 4.6H_2O\ (g) = 1.6V_V^* + 0.4Ti_V' + 4.6O_O^* + 0.2\square_{\ddot{O}} + 8HCl\ (g) + 0.6H_2(g) \qquad \text{(ii)}$$

The above proposed mechanism would result in an excess of n-type carriers further increasing the electronic conductivity of vanadium oxide. Furthermore, the doping of titanium into the vanadium oxide lattice also results in a shift of the d-band towards a more metallic state resulting in a further increase in electronic conductivity. This is reflected in Table 2, wherein both the VO_x: Ti-VACNT and VO_x-Ti have superior electronic conductivity of more than an order of magnitude in comparison to their undoped counterparts. This increase in electronic conductivity by doping with titanium would thus lead to enhanced inherent oxide electron transport and hence enhanced supercapacitor performance.

Table 2: Electronic conductivity data of various titanium doped vanadium oxide and undoped vanadium oxide and oxide-CNT composite electrodes.

Material	Resistivity (Ω-cm)
VO_x:Ti-VACNT	0.0182
VO_x-VACNT	0.46
VO_x:Ti	0.9
VO_x	7.5

Nickel current collector	$9.3 * 10^{-6}$

The marked improvement in electronic conductivity by serendipitous introduction of oxygen vacancies and Ti into the V_2O_5 oxide can be clearly demonstrated using first-principles computational approaches implemented for calculations of the electronic structure of the pure and doped vanadium oxide. Changes in the electronic structure of vanadium oxide with the introduction of oxygen vacancies and Ti-atoms in the oxide lattice results in substantial enhancement in the electronic conductivity of the material. For calculations of the total energy, density of electronic states and the cohesive energy (E_{coh} reflecting overall mechanical and chemical stability), the Vienna Ab-initio Simulation Package (VASP) based on the projector-augmented wave (PAW) formalism[108-110] within the generalized gradient approximation (GGA), for conducting the exchange-correlation corrections proposed by Perdew *et al.*[111], has been used in the present study. A plane-wave basis set with a cutoff energy of 520 eV and 184 *k*-points in the irreducible part of the Brillouin zone have been used to achieve an accuracy in the total energy of ~10^{-2} eV per formula unit, which is sufficient for a confident evaluation of the electronic structure, the cohesive energy and comparison of the results with corresponding experimental data.

V_2O_5 adopts an orthorhombic crystal structure with a space group D_{2h}^{13} - *Pmmn* (#59) with two formula units in the elementary unit cell. All structural parameters along with internal atomic Wyckoff positions are summarized in **Table 3** taken from the published report[112]. It should be noted, that there are three non-equivalent oxygen positions in the unit cell designated as bridge (O_b), vanadyl (O_v), and chain (O_c) oxygen sites.

Table 3: Crystal structure of V_2O_5[112]

Lattice constants (Å)		a = 11.512 Å	b = 3.564 Å	c = 4.368 Å
Atoms	Wyckoff positions	x	y	z
O_b	(2*a*)	0.0	0.0	0.001
O_v	(4*f*)	0.8543	0.0	0.531
O_c	(4*f*)	0.6811	0.0	0.003
V	(4*f*)	0.85118	0.0	0.8917

To simulate the experimentally studied materials, the following compounds have been constructed within one elementary unit cell containing 4 V and 10 O atoms: pure V_2O_5, $V_2O_{4.5}$ with one oxygen atom missing, and $V_{1.5}Ti_{0.5}O_{4.5}$ with one oxygen atom missing, and one V atom replaced for Ti. Such compositions although not exactly matching the actual experimentally generated systems, nevertheless could be very close approximations of the materials discussed in the present study: $V_2O_{4.6}$ and $V_{1.6}Ti_{0.4}O_{4.6}$. For $V_2O_{4.5}$ one vanadyl (O_v) atom has been removed to generate controlled defects, since previously there was shown in the computational study[113] that vanadyl vacancy at the O_v site is the most favored among all other possible sites in the vanadium pentoxide. Also, for Ti-doped $V_2O_{4.5}$ a vanadium atom next to the vanadyl vacancy has been replaced to create the Ti substitution. All the considered structures were fully relaxed with respect to change in volume, shape, and ion positions within a certain unit cell during the self-consistent energy minimization.

The total density of electronic states calculated for pure V_2O_5, $V_2O_{4.5}$ and $V_{1.5}Ti_{0.5}O_{4.5}$ are shown in **Figure 8** with the Fermi level E_F set for zero. One can see that V_2O_5 (**Figure 8a**) is a semiconductor with a forbidden energy gap between the valence and conduction zones. The valence band consists primarily of strongly hybridized oxygen 2p- and vanadium 3d- electronic

states with chiefly oxygen 2p-states, while the conduction band mainly consists of the vanadium 3d-states. This electronic structure correlates very well with results obtained in other theoretical studies previously published[113-115]. Our studies involving $V_2O_{4.5}$ and $V_{1.5}Ti_{0.5}O_{4.5}$ are unique however and provide new insight into the behavior of such doped structures. An internal analysis of the electronic structure showed that the valence band consisting primarily of O 2p states demonstrates a pronounced bonding character, while the conduction band comprises the anti-bonding states which was also noted in the work by Eyert et al.[114].

Figure 8b shows the total density of electronic states of $V_2O_{4.5}$. Since, one oxygen atom is missing, formally two vanadium 3d-electrons become free (unbounded) and thus fill the bottom of the previously empty conduction zone with these corresponding two electrons indeed rendering the material metallic. This phenomenon correlates well with results on the conductivity obtained in present study for $V_2O_{4.6}$ and discussed earlier.

Figure 8c demonstrates the total density of states for $V_{1.5}Ti_{0.5}O_{4.5}$. One can see that in general, the electronic structure is very similar to the previous case of $V_2O_{4.5}$ containing the oxygen vacancy with the only difference that now there is one Ti atom substituting in place of a V. Comparing these two cases it can be noted that although one oxygen vacancy releases two vanadium electrons in the unit cell, the introduction of a Ti atom bears one electron less than that of V, therefore contributing to only one electron per unit cell capable of conducting the electric charge through the material. Thus, $V_{1.5}Ti_{0.5}O_{4.5}$ still remains electronically conductive.

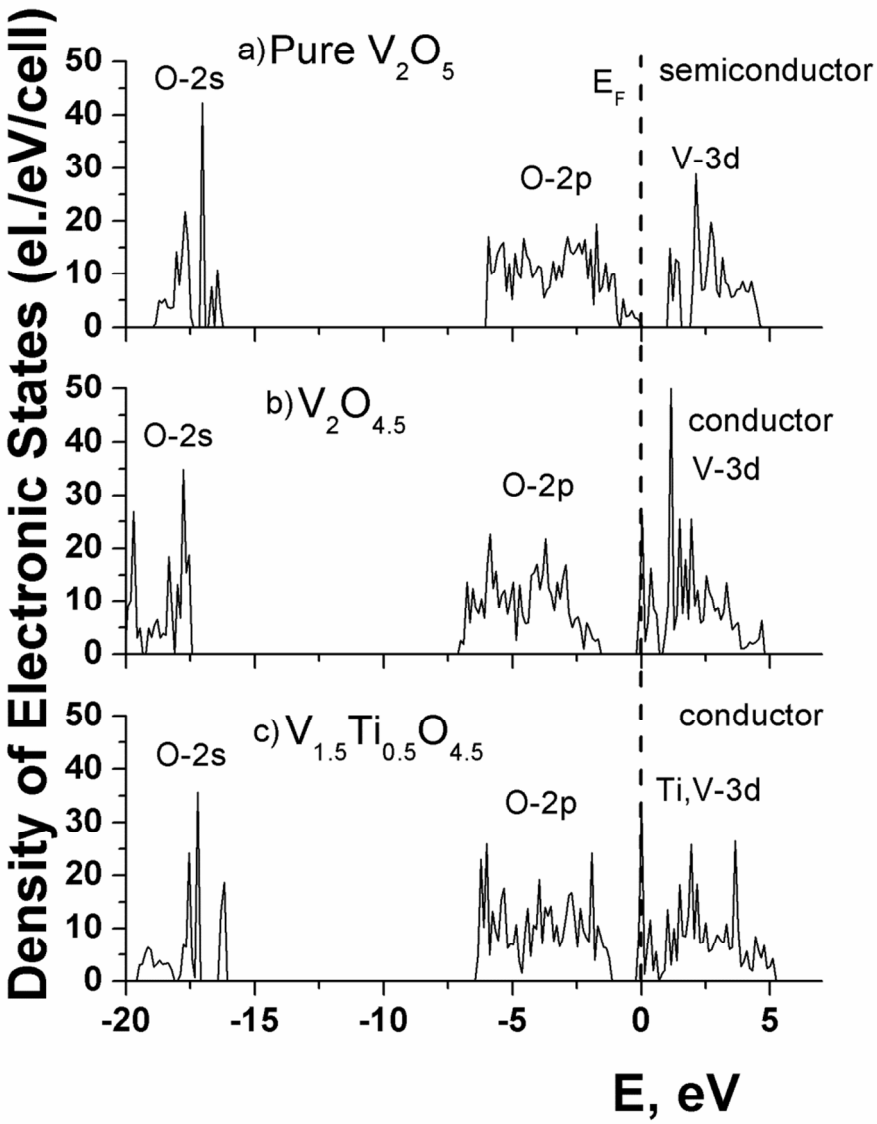

Figure 8: Total density of electronic states calculated for pure V_2O_5, $V_2O_{4.5}$ and $V_{1.5}Ti_{0.5}O_{4.5}$.

The metallic conductivity is usually proportional to the density of states at the Fermi level $n(E_F)$ and hence it provides an opportunity to qualitatively evaluate the electronic conductivity of $V_2O_{4.5}$ and $V_{1.5}Ti_{0.5}O_{4.5}$ oxides. For these purposes **Table 4** collects $n(E_F)$ for these materials showing that $n(E_F)$ calculated for $V_2O_{4.5}$ is lower than that corresponding to $V_{1.5}Ti_{0.5}O_{4.5}$. The

presence of Ti 3d-states increased to some extent the total density of states in the vicinity of the Fermi level thus rendering the material more electronically conductive than just the defective $V_2O_{4.5}$ oxide. This result is well confirmed by previously discussed experimental data summarized in **Table 2**.

Table 4: Comparison of density of states at Fermi energy level and cohesive energy between pure V_2O_5, vacancy-rich V_2O_5 and titanium doped vanadium oxide

Materials	**n(E_F), (el./(eV f.un.)**	**E_{coh} (eV/f.un.)**
V_2O_5	0 (band gap)	-42.17
$V_2O_{4.5}$	11.5	-39.05
$V_{1.5}Ti_{0.5}O_{4.5}$	15.5	-39.54

It should be noted that in this study the theoretical first principles analysis was used to explain the underlying phenomena resulting in superior electrical conductivity of the doped oxide materials. Although the first principles studies were performed on crystalline materials and not on the experimentally observed amorphous state though similar in composition, the results can nevertheless be considered as a qualitative representation of the behavior of amorphous materials corresponding to similar compositions. Amorphous materials as is known can be considered to be domains of short range periodicity not extending itself into the meso-scale state. Thus it can be hypothesized that the behavior of the larger body consisting of an infinite number of such domains would to some extent parallel the behavior of the domain itself. Though such a consideration is not perfect in the conventional and ideal sense, the experimental evidence nevertheless (**Table** 2) herein parallels the trends in electronic conductivity (**Table 4**), hence justifying the assumption to be valid at least for the case applicable to the present system.

Further, as mentioned above, the material should demonstrate high stability in the voltage of interest. For these purposes the cohesive energy E_{coh} can be considered a measure of an overall structural and chemical stability of the material. A higher E_{coh} would therefore imply that more energy is required to break the primary chemical bonds of the compound during chemical reaction. Thus, the cohesive energies of all three compounds considered in the present theoretical study have been calculated and summarized in **Table 4**.

From **Table 4** it can be construed that pure V_2O_5 is the most stable material in comparison with both the doped and defective oxides. It is therefore expected that the defective oxide with oxygen vacancies $V_2O_{4.5}$ would be less stable due to filling up of the anti-bonding electronic states in the conduction band above the band gap and also because of lowering the total number of V-O bonds in comparison with non-defective V_2O_5. Thus, presence of O-vacancies decreases the overall stability of the material to some extent. The situation albeit improves with the introduction of the Ti-doping. Because Ti-O bonds are stronger than V-O (668 kJ/mol vs. 637 kJ/mol bond strength in Ti-O and V-O diatomic molecules, respectively[116]) the overall stability of the Ti-doped vanadium oxide is higher than the undoped oxide.

Thus, in terms of the electronic conductivity and the overall stability the present theoretical study showcases $V_{1.5}Ti_{0.5}O_{4.5}$ as a promising super-capacitor material with excellent electrochemical properties. To the best of our knowledge, no theoretical studies exist correlating the effect of vacancies on the electronic structure of vanadium oxide and titanium oxide for supercapacitor applications. Based on the insight provided by this novel ab-initio study, we expect $V_{1.5}Ti_{0.5}O_{4.5}$ to be an excellent candidate for supercapacitor applications.

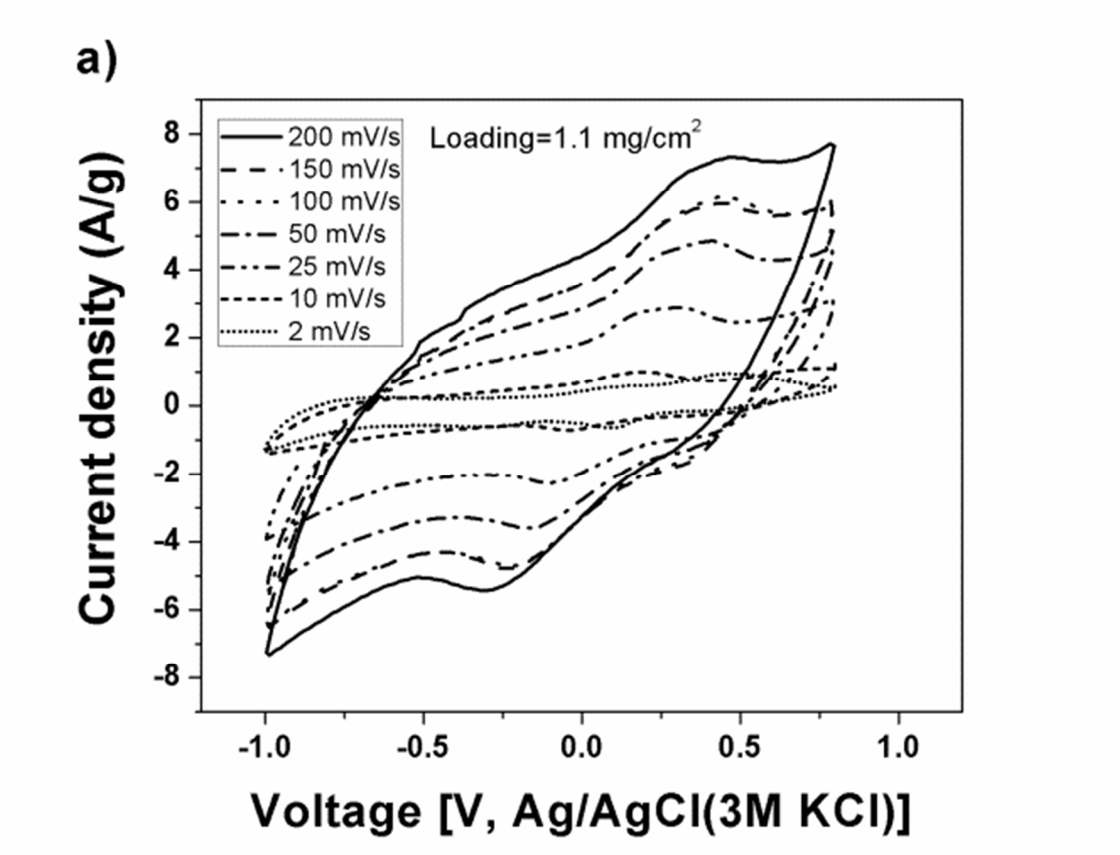

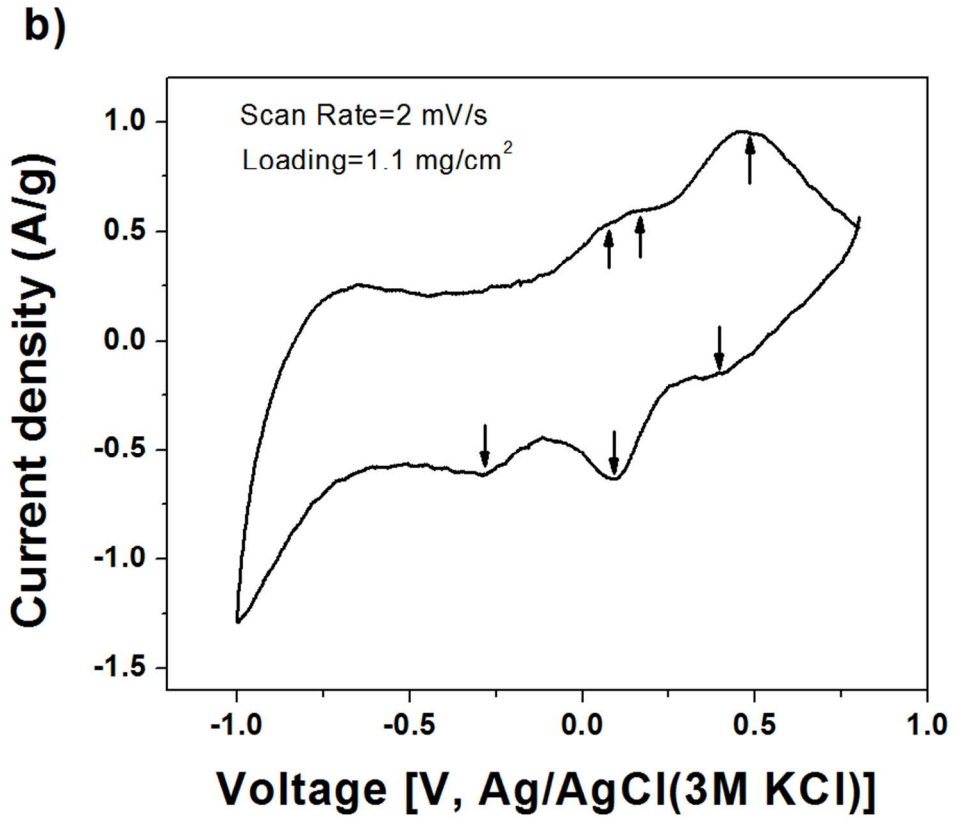

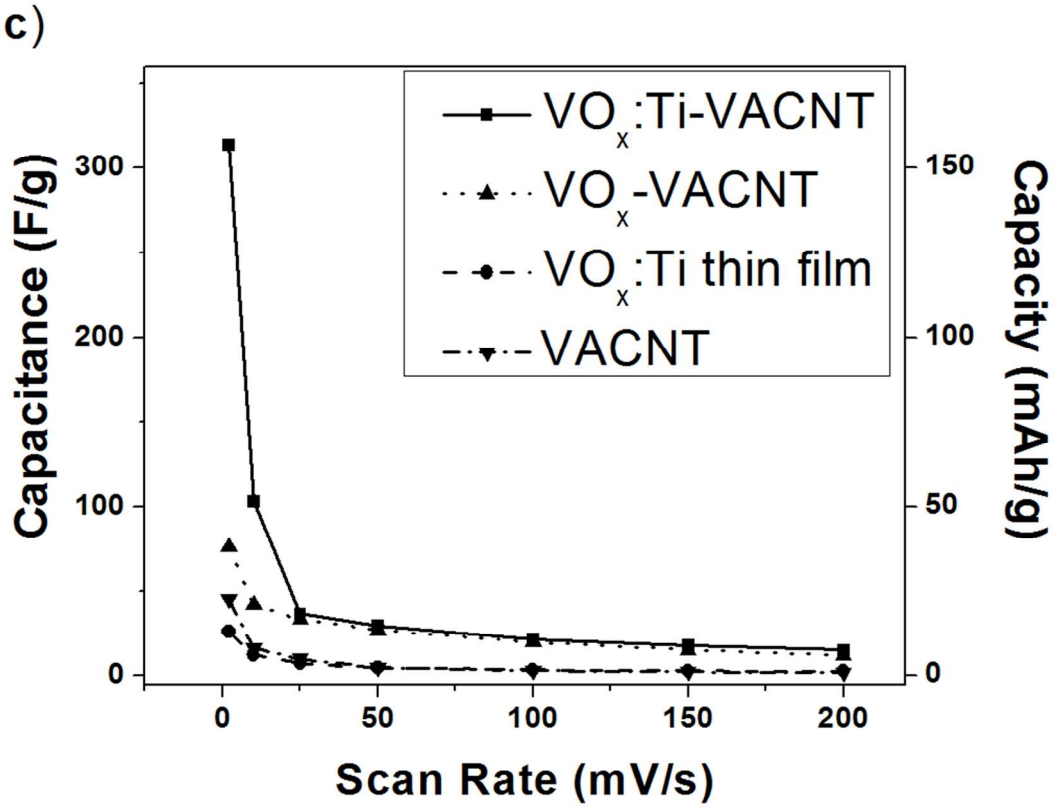

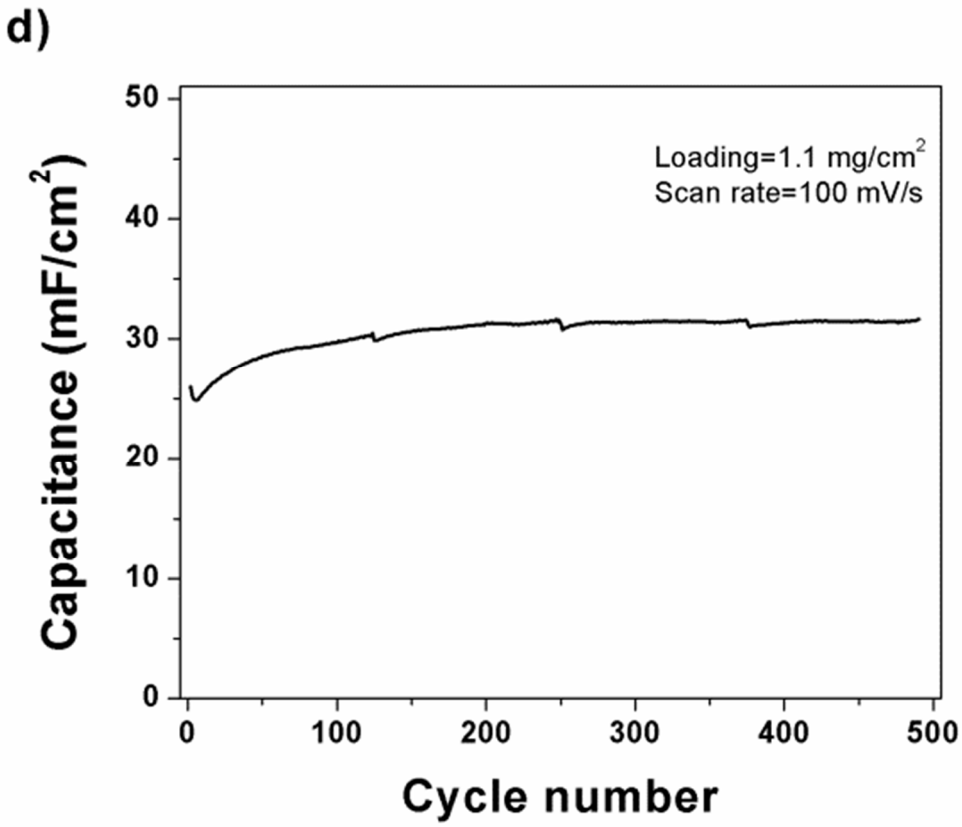

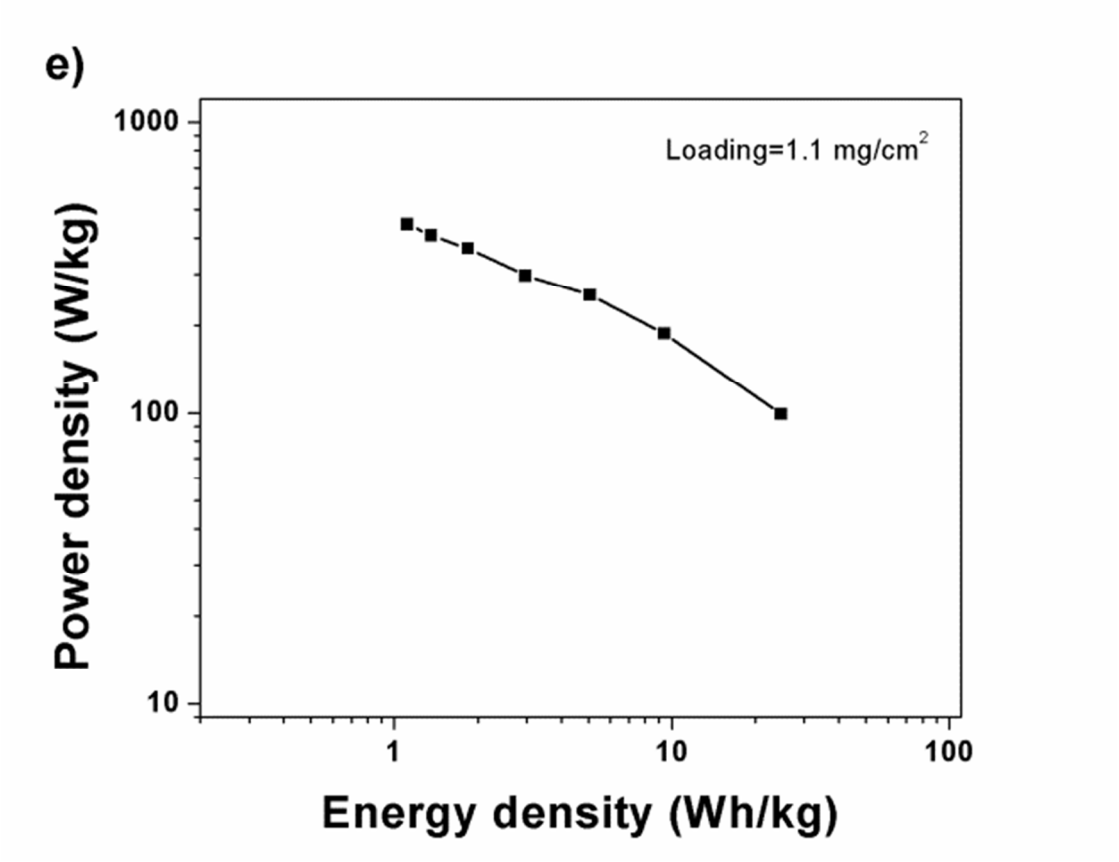

Figure 9: (a) Cyclic voltammograms of the VO_x:Ti-VACNT heterostructures at different scan rates, (b) Cyclic voltammograms of the VO_x:Ti-VACNT at 2mV/sec showing anodic and cathodic peaks for the reversible pseudocapacitive reactions, (c) Variation of capacitance with respect to scan rate for VO_x:Ti-VACNT , VO_x-VACNT and thin film VO_x-Ti (oxide loading=0.55 mg/cm^2, Oxide-VACNT active material loading=1.1 mg/cm^2) (d) Cycling data showing capacitance as a function of cycle number conducted at a scan rate of 100mV/sec, and (e) Ragone plot (power density *vs.* energy density) for VO_x:Ti-VACNT.

Figures 9a shows the cyclic voltammograms of the VO_x:Ti-VACNT at different scan rates ranging from 200mV/sec to 2mV/sec. The change in slopes of the I-V curves clearly shows the expected effects of scan rate. As the scan rate increases, the current response on scanning potential undergoes a transition from a flat capacitor type behavior to a resistor-like dependence as is common for most pseudocapacitor materials. The fade in capacitance with increase in scan rate is a phenomenon observed in all typical supercapacitor materials as described by Conway et.

al[6]. This is caused by the change in characteristic of the interface from that of a double layer capacitor to a typical resistor due to the inherent limitations and complexities of charge transfer and electron mobility dynamics.

It is well known that capacitance changes with scan rate, and is indeed a factor inherently dependent on the specific materials' characteristics. A similar characteristic in Faradaic reactions is the kinetic rate constant (k_o) which is a material property in a given electrode/electrolyte assembly. Pseudocapacitance reactions involving charge transfer by tunneling across the electrochemical interface have an inherent rate constant depending on the various species involved in the charge transfer which could be limiting in the case of the doped oxide coated on the CNTs. It is observed that even though the carbon nanotubes have a vertical alignment, the nature of the tethering of the oxide film on the carbon nanotubes needs to be improved to achieve better rate capability. Optimization of the system to improve the tethering of the doped oxide/VACNT and the CNT inherent conductivity would ideally increase both the initial capacitance as well as the rate capability, two of the most desired signatures characterizing the efficacy of a capacitor system. Such optimization studies are currently ongoing and will be reported in a forthcoming publication.

Figure 9b shows the slow scan rate cyclic voltammogram of the VO_x:Ti-VACNT composite electrode. Since voltammetry was performed at a slow rate, the Faradaic pseudocapacitance processes are hence not rate limited and distinct peaks occur corresponding to each Faradaic process is clearly visible. Reversible Faradaic peaks are observed at ~0.48V, 0.17V and 0.07V (*vs.* Ag/AgCl) on the positive scan and ~0.40V, 0.09V and -0.28V (*vs.* Ag/AgCl) on the negative scan in the VO_x:Ti-VACNT composite (see **Figure 9b and Table 5**). **Table 5** also shows tabulated the possible potential dependent pseudocapacitance type reactions

present at these potentials corresponding to a reversible transition of oxidation state of vanadium from +5 to +3, the most commonly observed in aqueous systems at the slightly alkaline pH (~8.5) occurring in a 1M Na_2SO_4 solution[117, 118]. In addition, the onset of water electrolysis is seen to occur at approximately, -0.75V (*vs.* Ag/AgCl) in **Figure 9b** at a low scan rate of 2 mV/s. This however is not observed at higher scan rates indicating that the kinetics of electrolysis are very sluggish on the VO_x:Ti-VACNT composite heterostructure electrodes, despite the improved electronic conductivity indicated in Table 2. We can therefore use this material over an extended window of ~1.8V with minimal or no electrolyte loss caused due to water electrolysis.

It should also be noted that in titanium oxide, the electronic state transition of Ti from +4 to +3 occurs generally around at ~-0.6V (vs. Ag/AgCl) at pH ~ 8.5[77, 78]. However, we can see that these transitions are not observed (see **Figure 9a** and **9b**) indicating that the titanium is completely doped into the VO_x lattice forming a solid solution with and no phase separation or secondary oxide formation. This further complements the Raman results confirming the Ti doping in the VO_x lattice.

Table 5: Faradaic charge transfer processes observed in the titanium doped vanadium oxide-VACNT composite electrode

Anodic scan peak potential (*vs.* Ag/AgCl)	**Cathodic scan peak potential (*vs.* Ag/AgCl)**	**Possible reaction mechanism**
~0.4839V	~0.3997V	$3V_2O_5\,(s) + 2H_2O + 4e^- \leftrightarrow V_6O_{13}\,(s) + 4OH^-$ $E = 0.8425 - 0.0591\times pH$ (Volts vs. SHE) $E = 0.1302$ (Volts vs. Ag/AgCl (3M KCl))
~0.1669V	~0.0922V	$V_6O_{13}\,(s) + H_2O + 2e^- \leftrightarrow 3V_2O_4\,(s) + 2OH^-$ $E = 0.4352 - 0.0591\times pH$ (Volts vs. SHE) $E = -0.2768$ (Volts vs. Ag/AgCl (3M KCl))

~0.074V	~-0.276V	$3V_2O_4\,(s) + 2H_2O + 4e^- \leftrightarrow 2V_3O_5\,(s) + 4OH^-$ $E = 0.3901 - 0.0591\times pH$ (Volts vs. SHE) $E = -0.3222$ (Volts vs. Ag/AgCl (3M KCl))

The variation of the capacitance of VO_x:Ti-VACNT, VO_x-VACNT and VO_x:Ti on Ni substrate with respect to scan rate is plotted in **Figure 9c** (oxide loading~0.55 mg/cm^2, oxide-VACNT loading~1.1 mg/cm^2) in addition to that of plain VACNT electrodes (used as a control). It should be noted that the capacitances of ~315 F/g (~157 mAh/g) shown in **Figure 9c** on the basis of the total active material loading (~1.1 mg/cm^2) (not just vanadium oxide loading) has been observed at a scan rate of 2 mV/s in the VO_x:Ti-VACNT nanocomposite material with excellent capacitance retention at higher rates. It can be seen that the VACNT electrode used as a control has a very low capacitance of ~45 F/g which drops with scan rate indicating that a very small part of the overall charge storage arises on account of the carbon nanotubes itself which is to be expected given that very small part of the CNTs are actually exposed to the electrolyte on account of being covered with the VO_x:Ti. The drop in capacitance with scan rate is due to the effect of the resistance/capacitance behavior previously described. Also, VO_x:Ti-VACNT has a higher capacitance not only at low scan rates but also at higher scan rates compared to VO_x: Ti thin film. In addition to capacitance, we have reported capacity in mAh/g for the various electrodes in **Figure 9c.** Vanadium oxide materials have previously been explored as charge storage electrodes in aqueous solutions in the form of aqueous batteries[110, 114]. However, it should be noted that the capacity obtained herein is almost twice that of previous studies wherein capacities of ~60-70 mAh/g have been reported with the electrode capacity rapidly fading to ~22

mAh/g over just a few cycles[119]. The areal capacitance for the VO_x:Ti-VACNT is between 350 $mFcm^{-2}$ and 30 $mFcm^{-2}$ (see **Figure 10**) which is superior to that reported for other supercapacitor materials at similar scan rates[120, 121]. The performance of supercapacitor materials at high rates is most-often limited by the electronic conductivity of the material. The presence of VACNTs as a support structure for the oxide leads to unidirectional electron transfer through the VACNTs[122] which then travel through the semi-contiguous film and interact at the oxide-electrolyte interface where the charge is stored. This allows for maximum CNT-oxide electron transport while minimizing electron transport through the VO_x grain boundaries which act as a barrier to electron transport. The present morphology also leads to increased surface exposure of the oxide to the electrolyte *i.e.* maximizing the electrochemical surface area and affording maximum exploitation of the capacitance behavior.

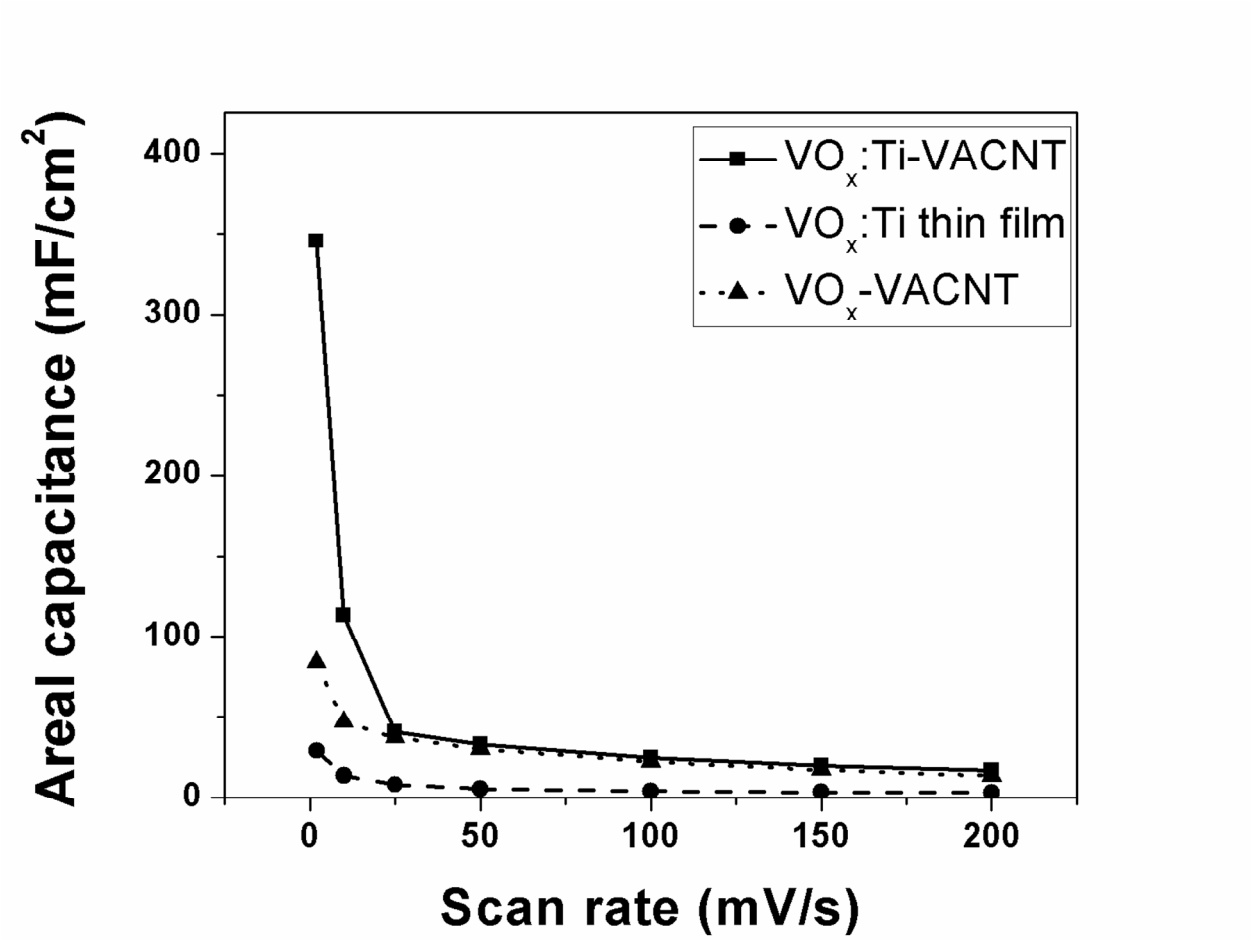

Figure 10: Variation of areal capacitance with respect to scan rate for VO_x:Ti-VACNT , VO_x-VACNT and thin film VO_x-Ti (oxide loading=0.55 mg/cm^2, Oxide-VACNT active material loading=1.1 mg/cm^2)

The cycling stability of the VO_x:Ti-VACNT supercapacitor material to retain charge over 400 cycles at a scan rate of 100mV/sec is shown in **Figure 9d**. Previous studies of vanadium oxide electrodes in aqueous electrolytes for charge storage have seldom yielded such superior electrochemical stability[119, 123].It can be observed that the areal capacitance increases initially stabilizing at a value of ~31 mF/cm^2. This excellent cyclability can be attributed to the reversible nature of the surface pseudocapacitance reactions of the oxide (see **Table 5**). The slight initial increase in capacity is possibly a result of the gradual improvement in wetting of the VO_x:Ti-

VACNT composite with the electrolyte. No significant difference is seen in the cycling behavior of VO_x-VACNT (previously reported by us[17]) and VO_x:Ti-VACNT reported herein indicating that both structures are stable in the electrolyte over the chosen voltage window. The oxidation state of the CVD deposited vanadium oxide is ~4.6 consisting predominantly of a +4/+5 oxide. According to the potential-pH diagram, at the pH of ~8.5, vanadium oxide has stable insoluble phases between the potentials of ~0.5 V and -1 V wrt Ag/AgCl[117]. Above 0.5 V, the higher oxidation state oxide is considered soluble to form $H_2VO_4^-$ at a neutral pH. This should be reflected as a loss in capacity with cycling. However, the onset potential of the electrochemical reactions is kinetically limited and is known to vary with particle size and the ensuing microstructure[124]. The Ti doped oxide is amorphous in the present work and most amorphous materials will be expected to exhibit lower stability compared to the crystalline counterpart due to the higher reactivity and defective state. However, the stronger Ti-O bonds and the overall higher cohesive energies for the crystalline counterpart translated to the amorphous state could likely contribute to the better stability of the system. Hence it is believed that the amorphous nature of the oxide nanoparticles supported on the vertically aligned carbon nanotubes could offset the onset of such dissolution resulting in the observed very stable performance of the oxide in aqueous Na_2SO_4 shown in **Figure 9d**. It is also possible that the kinetics of the dissolution reaction might be sluggish and such a fade in capacity would probably be observed if the material were cycled over several thousands of cycles which was not conducted in the present study since the objective was to demonstrate the performance of the doped system supported on VACNTs rather than demonstrate optimization of the system which will be part of the continued study that will be reported in subsequent publications. No post-cycling solution analysis was performed since significant fade was not observed over 500 cycles as seen in **Figure 9d**.

The synergistic effect of the carbon nanotube-vanadium oxide junction has previously been studied for gas-sensing purposes [95, 125, 126]. It has been suggested that a p-n junction type interaction between the VO_x and the CNT leads to increased catalytic response of the oxide while the multi walled CNTs, which acts as a p-type semiconductor facilitates the fast electron channels. A similar p-n type interaction can be expected to be observed in VO_x:Ti-VACNT composite as it is known that VO_x:Ti tends to exhibit predominantly n-type carrier behavior. All these factors are reflected in the improved electronic conductivity (**see Table 2**) contributing to achieving the improved rate capability, excellent supercapacitor response and cycling stability as seen in **Figure 9c and 9d**. Improved charge storage behavior may also be attributed to electronic sensitization of the doped oxide by this effect as commonly observed in doped oxides used for gas sensing applications[127].

It is common knowledge that thick films of nanoparticulate oxides especially amorphous oxides would be non-ideal configurations to obtain high capacitances on account of the low inherent electronic conductivity, grain boundary diffusion and exposed surface area. On the other hand, the use of a relatively thin film on a supported structure affords the benefits of high surface area, small particle size and direct contact of grains with the highly conductive carbon nanotube surface. This accessible capacitance of vanadium oxide is very much limited when the electrode is cast as a thick film. However, thin film titanium vanadium oxide has a high capacitance when supported on VACNTs as demonstrated in **Figure 9c**. The VACNTs act as a 3-dimensional electronically conductive support resulting in enhanced electrochemical surface area reflected both in the improved performance and rate capability of the VO_x:Ti-VACNT heterostructure composite. The overall capacitance reported in this manuscript is however lower than that reported in LiCl based systems by Hu et al.[26], as there is no intercalation mechanism involved in

tandem with the pseudocapacitance processes combined with double layer charge storage seen in the present VO_x:Ti-VACNT composite. Evaluation of VO_x:Ti-VACNT and other doped vanadium oxide systems is ongoing in intercalation based electrolytes and it is expected that higher energy density can be obtained using this system. The unique synthesis method, composition, morphology, electrode/electrolyte combination and an in-depth electrochemical characterization provided in this detailed study are original contributions enhancing the understanding of supercapacitor behavior in early transition metal oxide systems to the best of the understanding known from the published literature to date.

The above-stated improvements in the VOx:Ti-VACNT are reflected as the excellent supercapacitor performance seen in the Ragone plot (**Figure 9e**). The Ragone plot is conventionally used to represent the variation of energy density as a function of power density. An ideal device would maintain its energy density upon increasing power density. However, this is not very commonly observed as higher power densities indicate a greater diversion from equilibrium resulting in an L-shaped curve commonly seen showing higher power densities with low energy density and corresponding decrease in power densities with increasing energy density. In the case of the VO_x:Ti-VACNT high energy densities are sustained by the system with increasing power density although there is also observed a fade in energy density with rise in power density. The highest energy density of ~25 Wh/kg was obtained at a power density of ~100 W/kg. This is comparable to noble metal oxide (~25 Wh/kg) and very thin film based oxide (~30 Wh/kg) supercapacitor electrodes[128-130] and superior to other oxide materials(10-20 Wh/kg) representing the novelty of the work conducted in this study[131].

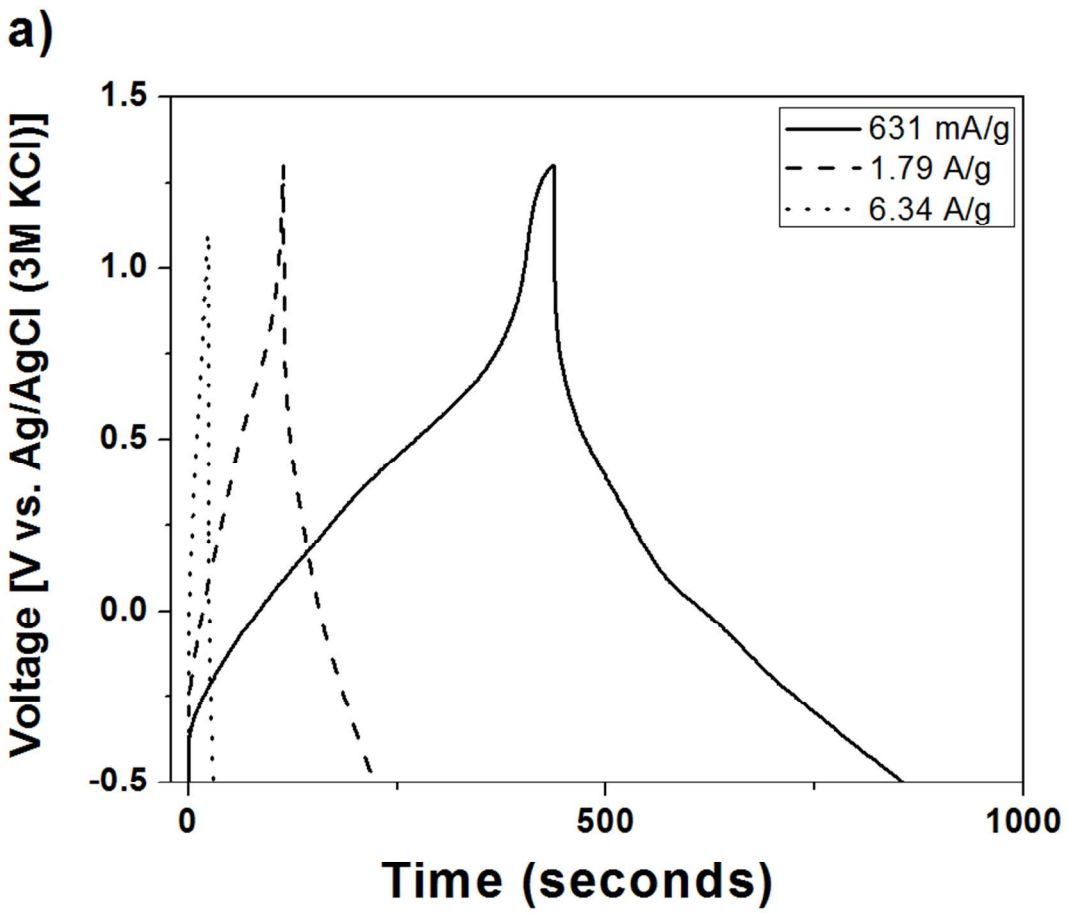

789

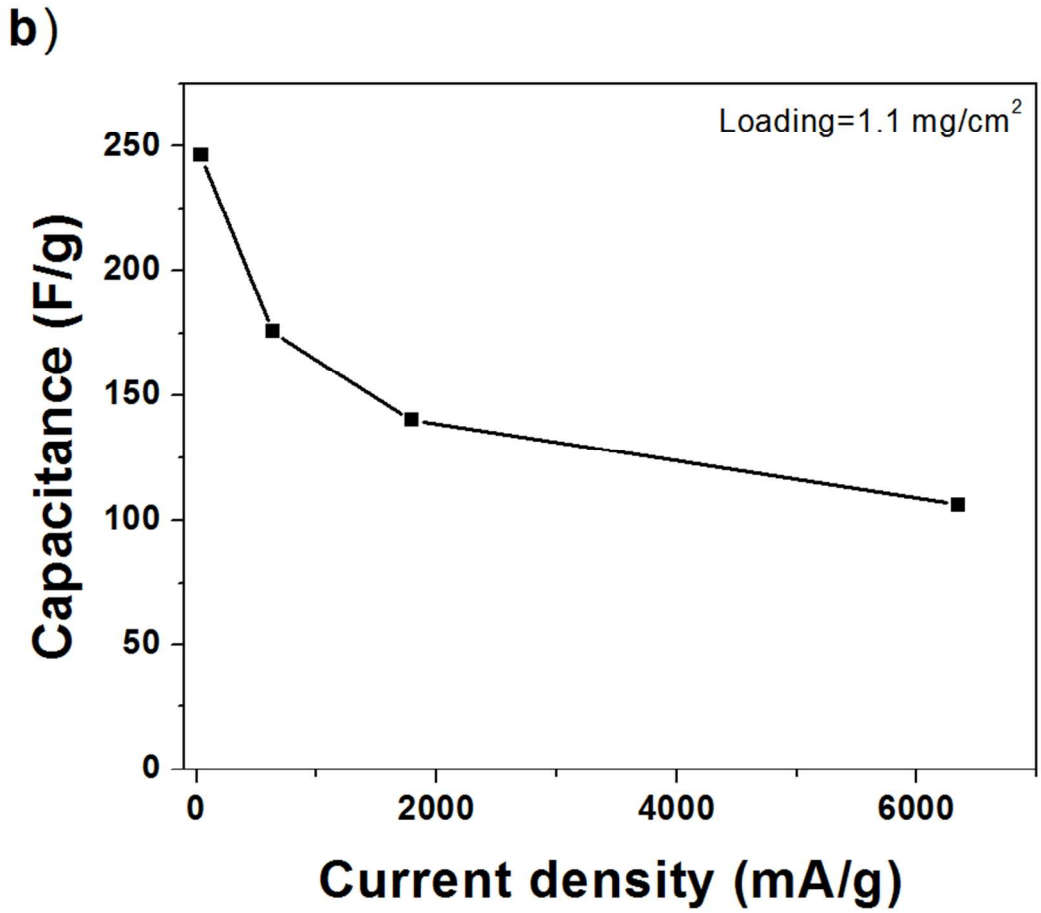

790

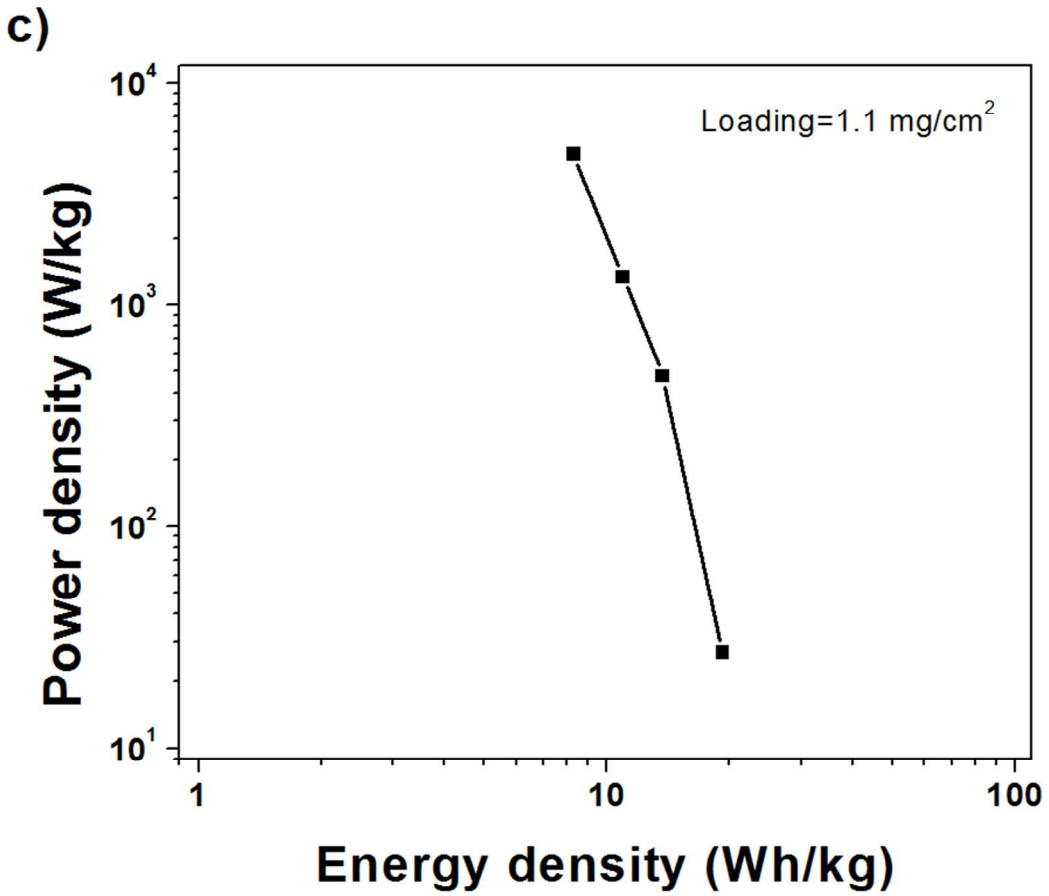

Figure 11: (a) Galvanostatic charge-discharge profiles of the VO_x:Ti-VACNT material (oxide loading=0.55 mg/cm^2, Oxide-VACNT active material loading=1.1 mg/cm^2) at different current densities (b) Capacitance dependence of the VO_x:Ti-VACNT material on current density calculated from the charge-discharge profiles in (a) (c) Ragone plot (power density vs. energy density) for VOx:Ti-VACNT calculated from the galvanostatic charge-discharge profiles.

Galvanostatic charge-discharge was performed on the most optimal material i.e. VO_x:Ti-VACNT in order to simulate the more practical commercial conditions and to examine the performance under high load. **Figure 11a** depicts the characteristic charge-discharge curves at different current densities. The material exhibits pseudocapacitor type behavior with very slight

shoulders at the potentials corresponding to the Faradaic reactions described in **Table 5**. It should be noted herein that the charge-discharge experiments were perfomed over a voltage window of -0.5 V to 1 V with respect to Ag/AgCl reference electrode. This was because onset of hydrogen evolution was found to occur at various potentials beyond ~-0.6 V depending on the current density. This was to be expected given that the window for water electrolysis is normally at 1.2 V. However, a stable reproducible charge-discharge behavior was observed over 1.5 V with no onset of electrolysis indicating that this material can be used over such an extended voltage window on account of the sluggish kinetics of electrolysis occurring on this material described earlier (**Figure 9b**). **Figure 11b** depicts the capacitance calculated from the charge-discharge profiles shown in **Figure 11a** as a function of current density. It can be seen that the VO_x:Ti-VACNT material exhibits high capacitance values of ~250 F/g at low scan rates which is retained very well even at higher scan rates. Capacitances of ~125 F/g are observed at very high current densities of ~6 A/g demonstrating the superior charge storage characteristics of the material as a result of the improved electronic conductivity and improved Faradaic reaction kinetics yielded by doping of the oxide as well as coating on the vertically aligned carbon nanotubes. The Ragone plot obtained from the galvanostatic charge-discharge data has been plotted in **Figure 11c**. Excellent energy densities of ~11 Wh/kg are retained at very high power densities of ~4.5 kW/kg, a demonstration of the excellent charge storage characteristics of the doped VO_x:Ti-VACNT material.

In order to further establish the advantages yielded by the CVD deposition of VO_x:Ti on VACNTs, electrochemical impedance spectroscopy (EIS) analysis was conducted on the nanospheres as well as the doped oxide film and charge transfer characteristics were accordingly compared. **Figures 12a** and **12b** show the Nyquist plots of the VO_x:Ti -VACNT hybrid and the

VO_x:Ti thin film oxide, respectively at different voltages over the window of interest. It can be directly observed that the impedance behavior of both materials is different especially at voltages close to the regions of the Faradaic peaks observed at ~0.48 V, 0.17 V and 0.07 V on the anodic scan and ~0.40 V, 0.09 V and -0.28 V in the cyclic voltammograms (see **Figure 9b**). At these potentials corresponding to the Faradaic charge transfer reactions, it can be seen upon comparing the response of VO_x:Ti and VO_x:Ti-VACNT composite that the thin film oxide has a much larger charge transfer resistance. This is inferred from the large semi-circular arcs seen in **Figure 12b** as compared to **Figure 12a** where one can see the Warburg tail being more prominent in **Figure 9a** as compared to the relatively much smaller semi-circular arcs (oxide loading~0.55 mg/cm^2, oxide-VACNT loading~1.1 mg/cm^2). The large semi-circular arcs in a Nyquist plot are indicative of high charge transfer resistance which would result in the reduced Faradaic response in VO_x:Ti thin film oxide at higher scan rates as seen in **Figure 9c**. Pseudocapacitance performance which is usually prevalent in the 10^3 to 10^4 Hz region on account of the electrode kinetic rate limitations[5] is much more prominent in the VO_x:Ti-VACNT as compared to the VO_x:Ti.

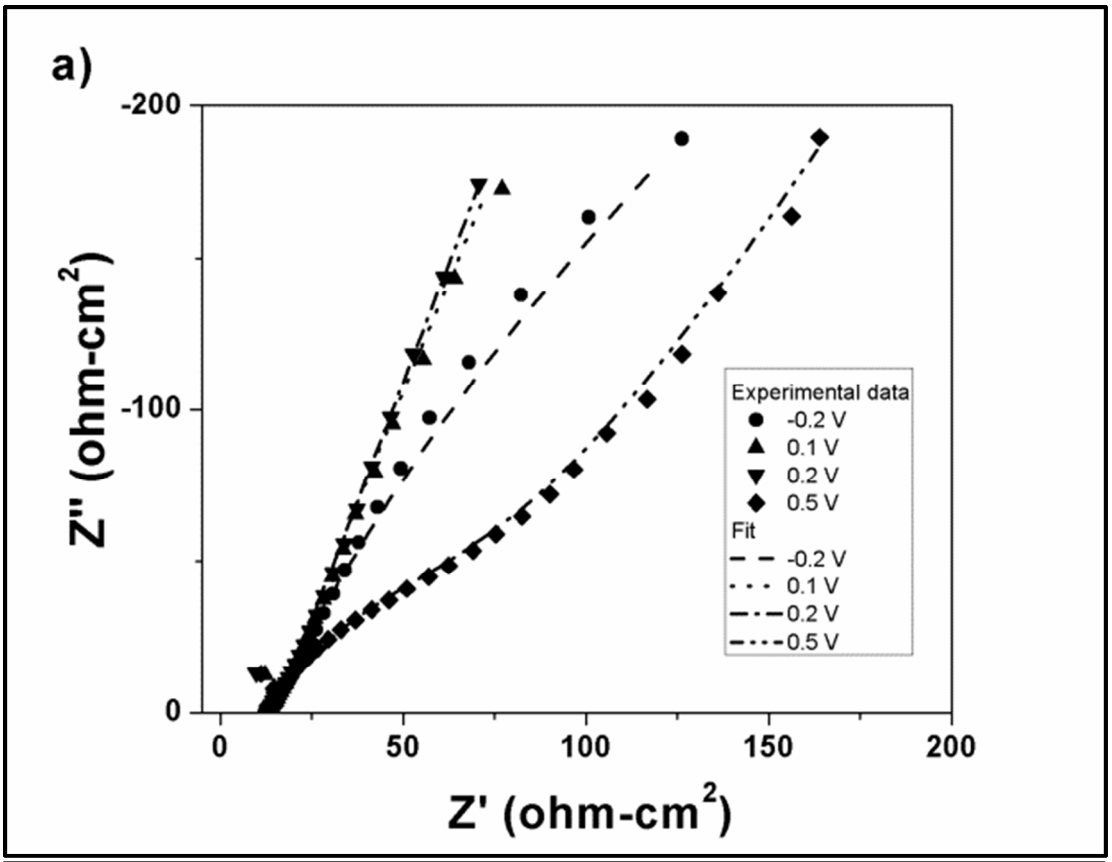

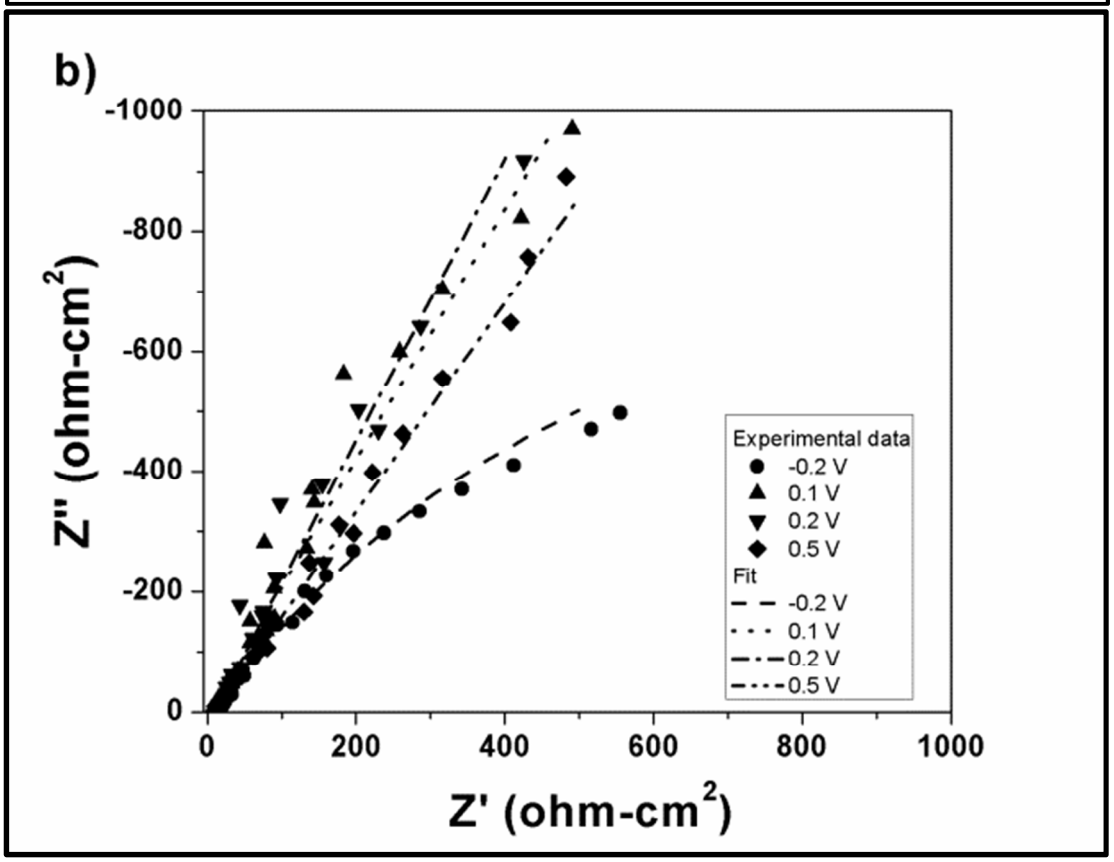

Figure 12: (a) Impedance behavior of VO_x:Ti-VACNT (oxide loading~0.55 mg/cm^2, oxide-VACNT loading~1.1 mg/cm^2) and (b) VO_x:Ti.

Equivalent Circuit modeling was performed using the Z-view software to obtain charge-transfer parameters of the titanium doped vanadium oxide thin film and titanium doped vanadium oxide-VACNT composite electrodes. An under-potential deposition mechanism described by Conway et. al.[5, 6] was used to model the pseudocapacitance reactions at both sets of electrodes. The mechanism considers both double layer capacitance (usually modeled as a capacitor (C_{dl}) in parallel with a resistor (R_F)) and pseudocapacitance arising from surface reactions (C_p) on the electrode of interest. In addition, an electrochemical series resistance (R_s) common to all electrochemical systems is also considered. However, in porous electrode systems, the capacitor elements are usually modeled as constant phase elements[7, 132]. Constant phase elements (CPE) are usually used to fit data having depressed semi-circular arcs on account of electrode porosity and roughness which leads to fractal character and inhomogeneity in response on account of presence of different crystallographic reaction sites. On account of such behavior noticeable in **Figures 12a and 12b**, we have used constant phase elements, CPE-dl and CPE-p to fit our data. The values of various charge transfer parameters obtained by fitting have been summarized in **Table 6**.

Table 6: Charge-transfer properties of the CVD derived titanium doped vanadium oxide materials.

Voltage	Series Resistance (R_s)-Ωcm^2		Double layer Constant Phase Element (CPE-dl)		Pseudocapacitance Constant phase element (CPE-F)		Faradaic resistance (R_F)-Ωcm^2	
	Ti-V oxid e-	Ti-V oxide thin	Ti-V oxide-VACNT composite	Ti-V oxide thin film	Ti-V oxide-VACNT composite	Ti-V oxide thin film	Ti-V oxide-VACNT	Ti-V oxide thin film

	VACNT composite	film	$T*10^4$	φ	$T*10^4$	φ	$T*10^4$	Φ	$T*10^4$	Φ	composite	
-0.2	2.46	1.67	6.14	0.86	4.22	0.60	23.37	0.71	0.24	0.98	0.86	9.68
0.1	2.51	1.7	3	0.98	0.04	0.96	19	0.77	1.17	0.72	0.94	1.06
0.2	2.51	1.69	6	0.90	0.05	0.94	16	0.77	1.01	0.73	1.44	1.09
0.5	2.46	2.01	23	0.74	0.57	0.84	56.95	0.71	1.11	0.75	24.06	37.83

It can be seen that the series resistance (R_s) is fairly constant in both systems and varies between 2 and 3 Ωcm^2 which is common in carbon based systems[133]. The most notable difference in behavior between VO_x:Ti and the VO_x:Ti-VACNT composite is the charge transfer resistance R_F. R_F values are reduced by up to an order on account of the presence of VACNTs. This can also be seen in **Figure 12a** where the oxide nanosphere-VACNT heterostructure based material has an almost 90 degree slope at low frequencies as compared to large semi-circles indicating high R_F values seen in **Figure 12b** [134]. R_F is the charge transfer resistance for electron tunneling from the electrode to the electrolyte i.e. the Faradaic pseudocapacitance process. R_F can usually be correlated with exchanged current density through the expression[5]:

$$R_F \text{ (in ohms)} = \frac{RT}{i_0 F} \qquad \text{iii)}$$

where

R= Gas constant (J/mol-K)

T= Temperature (in Kelvin)

i_0= Exchange current density (in Amperes)

F= Faraday constant (Coulomb/mol)

R_F as defined in **Equation iii** is the Faradaic charge-transfer resistance at reversible potential. A decrease in charge-transfer resistance thus indicates an increase in exchange current density resulting in increased rates of the Faradaic reactions. The value of R_F as defined in Equation iii is limited to the reversible potential of the particular reaction. Therefore, in addition to the above conclusion, one can understand that the Faradaic leakage current density and thus Faradaic charge-transfer resistance are overvoltage dependent[5]. The dependence of R_F on voltage can be seen in **Table 7**. **Table 7** compares the charge transfer resistance of the VO_x:Ti-VACNT with that of VO_x:Ti at different voltages and also to that of undoped VO_x thin film material prepared using a similar approach reported earlier[17]. The charge transfer resistance of VO_x:Ti – VACNT is less than or equal to that of VO_x:Ti at all the potentials indicating that electron tunneling across the electrochemical interface is more easily activated in the case of VO_x:Ti-VACNT than in the case of VO_x:Ti. The improvement in pseudocapacitance behavior can also be inferred by referring to the quantitative values of the constant phase elements (CPE-F) seen in **Table 6**. It can also be seen that there is an almost one order improvement in Faradaic charge-transfer resistance upon doping VO_x thin film material with titanium. The doping of titanium into the vanadium oxide lattice thus enhances not only the electronic conductivity but also the electrochemical performance to a certain extent resulting in the improved response displayed in **Figure 9c**. The presence of carbon nanotubes further enhances both the electronic conductivity and ease of electron transfer confirming that the VO_x:Ti –VACNT is indeed an excellent supercapacitor material.

Table 7: Comparison between the Faradaic charge-transfer resistance (R_F) (Ωcm^2) of the CVD derived VO_x:Ti and VO_x[17]

Voltage	**VO_x:Ti-VACNT**	**VO_x:Ti**	**Voltage**	**VO_x**

-0.2	0.86	9.68	-0.8	968.93
0.1	0.94	1.06	-0.3	58.802
0.2	1.44	1.09	0.2	58.197
0.5	24.06	37.83	0.3	67.12

Conclusions

Hot-wall chemical vapor deposition has for the first time been used to create a unique morphology consisting of titanium doped vanadium oxide nanospheres on vertically aligned carbon nanotubes (VACNTs). Such a CVD derived VO_x:Ti-VACNT heterostructured composite has been shown to exhibit excellent charge storage characteristics with capacitances of up to 313 F/g achieved at a scan rate of 2 mV/s particularly in a thick oxide nanosphere film coated on the VACNTs. The doping of titanium into the vanadium oxide lattice has been shown to have a salutary effect on the electrochemical charge storage capability of vanadium oxide due to the improved electronic conductivity, an essential parameter for achieving fast electron transport and charge transfer response. Another highlight of this study is the ease of electrode fabrication. Chemical vapor deposition (CVD) is a method amenable for continuous production of electrodes in an assembly-chain configuration in contrast with chemical methods used to produce oxides which is a batch process, and in-turn also involve a second heat treatment step. Moreover, the need for slurry preparation is eliminated and binder-free electrodes are thus generated. The formation of a thick film with high loadings (upto 1.1 mg/cm^2) by a chemical vapor deposition method allows for tailoring the morphology of the oxide, while also maintaining sufficient active materials resulting in high areal capacitance of upto ~350 mF/cm^2. The CVD method could

further be optimized to lead to electrodes with superior rate capability by tailoring the nature of the CNT-oxide interface by additional functionalization to attain better interface interaction and consequently, more improved electron transport. In addition, a complete survey of the titanium doped vanadium oxide capacitor behavior spectrum is in order and efforts are on to achieve the same, the results of which will be reported in subsequent manuscripts.

Acknowledgement

Research supported by the National Science Foundation, under Award CBET-0933141. PNK acknowledges the Edward R. Weidlein Chair Professorship funds and the Center for Complex Engineered Multifunctional Materials (CCEMM) for procuring the electrochemical equipment used in this research work. The authors would like to acknowledge the support of Dr. Susheng Tan, Nanoscale Fabrication and Characterization Facility at the University of Pittsburgh for help with Transmission Electron Microscopy data collection and analyses.

References

1. H. Chen, T. N. Cong, W. Yang, C. Tan, Y. Li and Y. Ding, *Progress in Natural Science*, 2009, 19, 291-312.
2. P. Jampani, A. Manivannan and P. N. Kumta, *Electrochemical Society Interface*, 2010, 19, 57-62.
3. U. S. A. B. Consortium, Department of Energy, 2006.
4. P. Simon and Y. Gogotsi, *Nature Materials*, 2008, 7, 845-854.
5. B. E. Conway, *Electrochemical Supercapacitors: Scientific Fundamentals and Technological Applications*, Kluwer Academic/Plenum Publishers, New York, 1999.
6. B. E. Conway, *J. Electrochem. Soc.*, 1991, 138, 1539-1548.
7. P. S. Germain, W. G. Pell and B. E. Conway, *Electrochim. Acta*, 2004, 49, 1775-1788.
8. C. C. Hu and T. W. Tsou, *Electrochemistry Communications*, 2002, 4, 105-109.
9. R. Kötz and M. Carlen, *Electrochimica Acta*, 2000, 45, 2483-2498.
10. J. M. Miller, B. Dunn, T. D. Tran and R. W. Pekala, *J. Electrochem. Soc.*, 1997, 144, L309-L311.
11. M. Toupin, T. Brousse and D. Belanger, *Chemistry of Materials*, 2002, 14, 3946-3952.
12. J. W. Long, K. E. Swider, C. I. Merzbacher and D. R. Rolison, *Langmuir*, 1999, 15, 780-785.
13. T. Kudo, Y. Ikeda, T. Watanabe, M. Hibino, M. Miyayama, H. Abe and K. Kajita, *Solid State Ionics*, 2002, 152, 833-841.
14. I. H. Kim, J. H. Kim, B. W. Cho, Y. H. Lee and K. B. Kim, *Journal of the Electrochemical Society*, 2006, 153, A989-A996.

15. S. D. Perera, B. Patel, J. Bonso, M. Grunewald, J. P. Ferraris and K. J. Balkus, *Acs Applied Materials & Interfaces*, 2011, 3, 4512-4517.
16. S. Tepavcevic, H. Xiong, V. R. Stamenkovic, X. Zuo, M. Balasubramanian, V. B. Prakapenka, C. S. Johnson and T. Rajh, *ACS Nano*, 2011, 6, 530-538.
17. P. H. Jampani, K. Kadakia, D. H. Hong, R. Epur, J. A. Poston, A. Manivannan and P. N. Kumta, *Journal of The Electrochemical Society*, 2013, 160, A1118-A1127.
18. W. Wang and P. N. Kumta, *Journal of Power Sources*, 2007, 172, 650-658.
19. I. Shakir, Z. Ali, J. Bae, J. Park and D. J. Kang, *Nanoscale*, 2014, 6, 4125-4130.
20. M. Lee, B. H. Wee and J. D. Hong, *Advanced Energy Materials*, 2014.
21. H. Wang, H. Yi, X. Chen and X. Wang, *Journal of Materials Chemistry A*, 2014, 2, 1165-1173.
22. M. E. Spahr, P. Bitterli, R. Nesper, M. Muller, F. Krumeich and H. U. Nissen, *Angewandte Chemie-International Edition*, 1998, 37, 1263-1265.
23. M. E. Spahr, P. Stoschitzki-Bitterli, R. Nesper, O. Haas and P. Novak, *Journal of the Electrochemical Society*, 1999, 146, 2780-2783.
24. C. C. Hu, C. M. Huang and K. H. Chang, *Journal of Power Sources*, 2008, 185, 1594-1597.
25. C. M. Huang, C. C. Hu, K. H. Chang, J. M. Li and Y. F. Li, *J. Electrochem. Soc.*, 2009, 156, A667-A671.
26. J. M. Li, K. H. Chang and C. C. Hu, *Electrochemistry Communications*, 2010, 12, 1800-1803.
27. J. M. Li, K. H. Chang, T. H. Wu and C. C. Hu, *Journal of Power Sources*, 2013, 224, 59-65.
28. M. E. Franke, T. J. Koplin and U. Simon, *Small*, 2006, 2, 36-50.
29. G. Korotcenkov, *Sensors and Actuators B: Chemical*, 2005, 107, 209-232.
30. Y. Wei, C.-W. Ryu and K.-B. Kim, *Journal of Power Sources*, 2007, 165, 386-392.
31. D. Hara, H. Ikuta, Y. Uchimoto and M. Wakihara, *Journal of Materials Chemistry*, 2002, 12, 2507-2512.
32. H. K. Park, *Solid State Ionics*, 2005, 176, 307-312.
33. L. Q. Mai, W. Chen, Q. Xu, J. F. Peng and Q. Y. Zhu, *Chem. Phys. Lett.*, 2003, 382, 307-312.
34. K. Kadakia, M. K. Datta, P. H. Jampani, S. K. Park and P. N. Kumta, *Journal of Power Sources*, 2013, 222, 313-317.
35. K. Kadakia, M. K. Datta, O. I. Velikokhatnyi, P. Jampani, S. K. Park, P. Saha, J. A. Poston, A. Manivannan and P. N. Kumta, *International Journal of Hydrogen Energy*, 2012, 37, 3001-3013.
36. F. Coustier, J. Hill, B. B. Owens, S. Passerini and W. H. Smyrl, *J. Electrochem. Soc.*, 1999, 146, 1355-1360.
37. F. Coustier, S. Passerini and W. H. Smyrl, *Solid State Ionics*, 1997, 100, 247-258.
38. Y. Takasu, S. Mizutani, M. Kumagai, S. Sawaguchi and Y. Murakami, *Electrochemical and Solid State Letters*, 1999, 2, 1-2.
39. E. Frackowiak and F. Béguin, *Carbon*, 2001, 39, 937-950.
40. E. Frackowiak, K. Metenier, V. Bertagna and F. Beguin, *Appl. Phys. Lett.*, 2000, 77, 2421-2423.

41. P. Kurzweil, in *Encyclopedia of Electrochemical Power Sources*, ed. G. Editor-in-Chief: Jürgen, Elsevier, Amsterdam, 2009, DOI: 10.1016/b978-044452745-5.00352-x, pp. 634-648.
42. S. Stankovich, D. A. Dikin, G. H. B. Dommett, K. M. Kohlhaas, E. J. Zimney, E. A. Stach, R. D. Piner, S. T. Nguyen and R. S. Ruoff, *Nature*, 2006, 442, 282-286.
43. S. Stankovich, D. A. Dikin, R. D. Piner, K. A. Kohlhaas, A. Kleinhammes, Y. Jia, Y. Wu, S. T. Nguyen and R. S. Ruoff, *Carbon*, 2007, 45, 1558-1565.
44. A. K. Geim and K. S. Novoselov, *Nature Materials*, 2007, 6, 183-191.
45. K. S. Novoselov, A. K. Geim, S. V. Morozov, D. Jiang, Y. Zhang, S. V. Dubonos, I. V. Grigorieva and A. A. Firsov, *Science*, 2004, 306, 666-669.
46. S. Murali, J. R. Potts, S. Stoller, J. Park, M. D. Stoller, L. L. Zhang, Y. Zhu and R. S. Ruoff, *Carbon*, 2012, 50, 3482-3485.
47. Y. Zhu, S. Murali, M. D. Stoller, K. J. Ganesh, W. Cai, P. J. Ferreira, A. Pirkle, R. M. Wallace, K. A. Cychosz, M. Thommes, D. Su, E. A. Stach and R. S. Ruoff, *Science*, 2011, 332, 1537-1541.
48. Z. Chen, V. Augustyn, X. L. Jia, Q. F. Xiao, B. Dunn and Y. F. Lu, *ACS Nano*, 2012, 6, 4319-4327.
49. Q. W. Li, Y. Li, X. F. Zhang, S. B. Chikkannanavar, Y. H. Zhao, A. M. Dangelewicz, L. X. Zheng, S. K. Doorn, Q. X. Jia, D. E. Peterson, P. N. Arendt and Y. T. Zhu, *Advanced Materials*, 2007, 19, 3358-3363.
50. P. L. McEuen, M. S. Fuhrer and H. K. Park, *IEEE Trans. Nanotechnol.*, 2002, 1, 78-85.
51. T. W. Odom, J.-L. Huang, P. Kim and C. M. Lieber, *Nature*, 1998, 391, 62-64.
52. P. Ajayan, *Chemical reviews*, 1999, 99, 1787-1800.
53. J. W. G. Wilder, L. C. Venema, A. G. Rinzler, R. E. Smalley and C. Dekker, *Nature*, 1998, 391, 59-62.
54. T. Szorenyi, K. Bali and I. Hevesi, *Journal of Non-Crystalline Solids*, 1980, 35-6, 1245-1248.
55. S. D. Perera, B. Patel, N. Nijem, K. Roodenko, O. Seitz, J. P. Ferraris, Y. J. Chabal and K. J. Balkus, *Advanced Energy Materials*, 2011, 1, 936-945.
56. C. Y. Lee, H. M. Tsai, H. J. Chuang, S. Y. Li, P. Lin and T. Y. Tseng, *Journal of the Electrochemical Society*, 2005, 152, A716-A720.
57. A. L. M. Reddy, M. M. Shaijumon, S. R. Gowda and P. M. Ajayan, *Nano Letters*, 2009, 9, 1002-1006.
58. S. R. Sivakkumar, J. M. Ko, D. Y. Kim, B. C. Kim and G. G. Wallace, *Electrochimica Acta*, 2007, 52, 7377-7385.
59. Z. Fan, J. Chen, K. Cui, F. Sun, Y. Xu and Y. Kuang, *Electrochimica Acta*, 2007, 52, 2959-2965.
60. I. H. Kim, J. H. Kim and K. B. Kim, *Electrochemical and Solid State Letters*, 2005, 8, A369-A372.
61. I. H. Kim, J. H. Kim, Y. H. Lee and K. B. Kim, *Journal of the Electrochemical Society*, 2005, 152, A2170-A2178.
62. S. D. Perera, B. Patel, N. Nijem, K. Roodenko, O. Seitz, J. P. Ferraris, Y. J. Chabal and K. J. Balkus, *Advanced Energy Materials*, 2011, 1, 936-945.
63. M. Sathiya, A. S. Prakash, K. Ramesha, J. M. Tarascon and A. K. Shukla, *J. Am. Chem. Soc.*, 2011, 133, 16291-16299.

64. Z. Chen, Y. C. Qin, D. Weng, Q. F. Xiao, Y. T. Peng, X. L. Wang, H. X. Li, F. Wei and Y. F. Lu, *Adv. Funct. Mater.*, 2009, 19, 3420-3426.
65. D. Choi, G. E. Blomgren and P. N. Kumta, *Advanced Materials*, 2006, 18, 1178-+.
66. Y. Gogotsi and P. Simon, *Science*, 2011, 334, 917-918.
67. J. C. Badot and N. Baffier, *Journal of Materials Chemistry*, 1992, 2, 1167-1174.
68. Y. Wang and G. Cao, *Chemistry of Materials*, 2006, 18, 2787-2804.
69. S. Boukhalfa, K. Evanoff and G. Yushin, *Energy & Environmental Science*, 2012, 5, 6872-6879.
70. N. Ozer, S. Sabuncu and J. Cronin, *Thin Solid Films*, 1999, 338, 201-206.
71. W. Wang, R. Epur and P. N. Kumta, *Electrochemistry Communications*, 2011, 13, 429-432.
72. W. Wang and P. N. Kumta, *ACS Nano*, 2010, 4, 2233-2241.
73. D. Vernardou, P. Paterakis, H. Drosos, E. Spanakis, I. M. Povey, M. E. Pemble, E. Koudoumas and N. Katsarakis, *Solar Energy Materials and Solar Cells*, 2011, 95, 2842-2847.
74. L. Michailovits, K. Bali, T. Szorenyi and I. Hevesi, *Acta Physica Academiae Scientiarum Hungaricae*, 1980, 49, 217-221.
75. R. Binions, G. Hyett, C. Piccirillo and I. P. Parkin, *Journal of Materials Chemistry*, 2007, 17, 4652-4660.
76. T. D. Manning and I. P. Parkin, *Polyhedron*, 2004, 23, 3087-3095.
77. M. N. Field and I. P. Parkin, *Journal of Materials Chemistry*, 2000, 10, 1863-1866.
78. T. D. Manning, I. P. Parkin, R. J. H. Clark, D. Sheel, M. E. Pemble and D. Vernadou, *Journal of Materials Chemistry*, 2002, 12, 2936-2939.
79. I. P. Parkin and G. S. Elwin, *Journal of Materials Chemistry*, 2001, 11, 3120-3124.
80. S. K. Pal, S. Talapatra, S. Kar, L. Ci, R. Vajtai, T. Borca-Tasciuc, L. S. Schadler and P. M. Ajayan, *Nanotechnology*, 2008, 19.
81. S. Talapatra, S. Kar, S. K. Pal, R. Vajtai, L. Ci, P. Victor, M. M. Shaijumon, S. Kaur, O. Nalamasu and P. M. Ajayan, *Nature Nanotechnology*, 2006, 1, 112-116.
82. T. D. Manning, I. P. Parkin, M. E. Pemble, D. Sheel and D. Vernardou, *Chem. Mat.*, 2004, 16, 744-749.
83. C. S. Blackman, C. Piccirillo, R. Binions and I. P. Parkin, *Thin Solid Films*, 2009, 517, 4565-4570.
84. D. Vernardou, M. E. Pemble and D. W. Sheel, *Chemical Vapor Deposition*, 2007, 13, 158-162.
85. C. Emmenegger, J. M. Bonard, P. Mauron, P. Sudan, A. Lepora, B. Grobety, A. Zuttel and L. Schlapbach, *Carbon*, 2003, 41, 539-547.
86. G. Atthipalli, R. Epur, P. N. Kumta, M. Yang, J. K. Lee and J. L. Gray, *J. Phys. Chem. C*, 2011, 115, 3534-3538.
87. M. Sathiya, A. S. Prakash, K. Ramesha, J. M. Tarascon and A. K. Shukla, *Journal of the American Chemical Society*, 2011, 133, 16291-16299.
88. E. Hryha, E. Rutqvist and L. Nyborg, *Surface and Interface Analysis*, 2012, 44, 1022-1025.
89. A. V. Naumkin, A. Kraut-Vass, S. W. Gaarenstroom and C. J. Powell, in *NIST Standard Reference database 20*, National Institute of Standards & Technology, 2012, vol. Version 4.1.

90. N. I. S. Testing, http://srdata.nist.gov/xps/elm_Spectra_query.aspx?Elm1=V&LD1=2p1%2f2&Elm2=V&LD2=2p3%2f2&Elm3=&LD3=&Elm4=&LD4=&sType=PE, Accessed 11/24/2014, 2014.
91. V. L. Volkov, G. S. Zakharova, E. G. Volkova and M. V. Kuznetsov, *Russ. J. Inorg. Chem.*, 2006, 51, 847-851.
92. A. C. Ferrari and J. Robertson, *Phys. Rev. B*, 2000, 61, 14095-14107.
93. A. C. Ferrari and J. Robertson, *Phys. Rev. B*, 2001, 64.
94. E. Cazzanelli, G. Mariotto, S. Passerini, W. H. Smyrl and A. Gorenstein, *Solar Energy Materials and Solar Cells*, 1999, 56, 249-258.
95. S. Santangelo, G. Messina, G. Faggio, M. G. Willinger, N. Pinna, A. Donato, A. Arena, N. Donato and G. Neri, *Diamond and Related Materials*, 2010, 19, 590-594.
96. A. Löfberg, T. Giornelli, S. Paul and E. Bordes-Richard, *Applied Catalysis A: General*, 2011, 391, 43-51.
97. M. G. Nobbenhuis, A. Baiker, P. Barnickel and A. Wokaun, *Applied Catalysis A: General*, 1992, 85, 157-172.
98. H. Liu, Y. Wu and J. Zhang, *Acs Applied Materials & Interfaces*, 2011, 3, 1757-1764.
99. V. Stengl, D. Popelkova and P. Vlacil, *J. Phys. Chem. C*, 2011, 115, 25209-25218.
100. G. N. Kryukova, G. A. Zenkovets, G. Mestl and R. Schlogl, *Reaction Kinetics and Catalysis Letters*, 2003, 80, 161-169.
101. G. T. Went, S. T. Oyama and A. T. Bell, *J. Phys. Chem.*, 1990, 94, 4240-4246.
102. N. Y. Topsoe, M. Anstrom and J. A. Dumesic, *Catal. Lett.*, 2001, 76, 11-20.
103. J. B. MacChesney and H. J. Guggenheim, *Journal of Physics and Chemistry of Solids*, 1969, 30, 225-234.
104. J. Muster, G. T. Kim, V. Krstic, J. G. Park, Y. W. Park, S. Roth and M. Burghard, *Advanced Materials*, 2000, 12, 420-+.
105. L. A. Balagurov, I. V. Kulemanov, A. F. Orlov and E. A. Petrova, *Russ Microelectron*, 2012, 41, 503-507.
106. N. Serpone, D. Lawless, J. Disdier and J.-M. Herrmann, *Langmuir*, 1994, 10, 643-652.
107. J. D. Butler, *Transactions of the Faraday Society*, 1960, 56, 1842-1850.
108. G. Kresse and J. Furthmüller, *Physical Review B*, 1996, 54, 11169-11186.
109. G. Kresse and J. Furthmüller, *Computational Materials Science*, 1996, 6, 15-50.
110. G. Kresse and D. Joubert, *Physical Review B*, 1999, 59, 1758-1775.
111. J. P. Perdew and W. Yue, *Physical Review B*, 1986, 33, 8800-8802.
112. R. Enjalbert and J. Galy, *Acta Crystallographica Section C*, 1986, 42, 1467-1469.
113. S. Laubach, P. C. Schmidt, Thi, F. J. Fernandez-Madrigal, Q.-H. Wu, W. Jaegermann, M. Klemm and S. Horn, *Physical Chemistry Chemical Physics*, 2007, 9, 2564-2576.
114. V. Eyert and K. H. Höck, *Physical Review B*, 1998, 57, 12727-12737.
115. A. Chakrabarti, K. Hermann, R. Druzinic, M. Witko, F. Wagner and M. Petersen, *Physical Review B*, 1999, 59, 10583-10590.
116. D. R. Lide, *CRC Handbook of chemistry and physics, 86th edn, 2005–2006*, CRC Press, Boca Raton, 2005.
117. M. Pourbaix, *Atlas of electrochemical equilibria in aqueous solutions*, Pergamon Press, Oxford, 1966.
118. N. Takeno, *Atlas of Eh-pH diagrams*, National Institute of Advanced Industrial Science & Technology, 2005.

119. S. Zhang, Y. Li, C. Wu, F. Zheng and Y. Xie, *The Journal of Physical Chemistry C*, 2009, 113, 15058-15067.
120. H. Kim and B. N. Popov, *Journal of Power Sources*, 2002, 104, 52-61.
121. G. Zheng, L. Hu, H. Wu, X. Xie and Y. Cui, *Energy & Environmental Science*, 2011, 4, 3368-3373.
122. M. Zhang, M. Yudasaka, S. Bandow and S. Iijima, *Chem. Phys. Lett.*, 2003, 369, 680-683.
123. H. Q. Yang, D. P. Li, S. Han, N. Li and B. X. Lin, *Journal of Power Sources*, 1996, 58, 221-224.
124. D. Choi, Doctor of Philosophy, Carnegie Mellon University, 2005.
125. M.-G. Willinger, G. Neri, A. Bonavita, G. Micali, E. Rauwel, T. Herntrich and N. Pinna, *Physical Chemistry Chemical Physics*, 2009, 11, 3615-3622.
126. L. Niinisto, M. Ritala and M. Leskela, *Mater. Sci. Eng. B-Solid State Mater. Adv. Technol.*, 1996, 41, 23-29.
127. A. Ponzoni, E. Comini, I. Concina, M. Ferroni, M. Falasconi, E. Gobbi, V. Sberveglieri and G. Sberveglieri, *Sensors*, 2012, 12, 17023-17045.
128. J. M. Sieben, E. Morallón and D. Cazorla-Amorós, *Energy*, 2013, 58, 519-526.
129. X. Liu and P. G. Pickup, *Journal of Power Sources*, 2008, 176, 410-416.
130. N. Nagarajan, M. Cheong and I. Zhitomirsky, *Materials Chemistry and Physics*, 2007, 103, 47-53.
131. Y. J. Kang, H. Chung and W. Kim, *Synthetic Metals*, 2013, 166, 40-44.
132. G. J. Brug, A. L. G. Vandeneeden, M. Sluytersrehbach and J. H. Sluyters, *Journal of Electroanalytical Chemistry*, 1984, 176, 275-295.
133. C. Portet, G. Yushin and Y. Gogotsi, *Carbon*, 2007, 45, 2511-2518.
134. V. Subramanian, H. W. Zhu and B. Q. Wei, *Electrochemistry Communications*, 2006, 8, 827-832.